Final Report **USDOE DE-FG02-88ER40414**
DOE Office of Science
Office of Nuclear Physics (Low Energy)
Dr. Cyrus Baktash, Program Manager

STUDIES OF HEAVY-ION REACTIONS AND TRANSURANIC NUCLEI

W. Udo Schröder

Principal Investigator

Departments of Chemistry and Physics
University of Rochester, Rochester, New York 14627

Grant Period

April 1, 2013 - March 31, 2016

Executive Summary

Studies of heavy-ion reactions and transuranic nuclei performed by the University of Rochester Nuclear Science Research Group have been successful in furthering experimental systematics and theoretical understanding of the behavior of nuclear systems excited to their limits of stability. The theoretical results explain specifically the “boiling” and “vaporization” of atomic nuclei but are more generally applicable to isolated, quantal many-particle systems which, under thermal or mechanical stresses, all disintegrate by evaporation, via surface cluster emission, or via fission-like processes.

Accompanying experimental investigations by the group have demonstrated several new types of dynamical instability of nuclei: In central, “head-on” collisions, target nuclei exhibit limited ability to stop energetic projectile nuclei and to dissipate the imparted linear momentum. Substantial matter overlap (“neck”) between projectile and target nuclei, which is observed at elevated collision energies, can be stretched considerably and break at several places simultaneously. These results provide new testing grounds for microscopic theory of the cohesion of nuclear matter. This property has remained elusive, even though the elementary nucleon-nucleon forces are well known since some time.

Technical R&D has resulted in a detailed characterization of a novel plastic material, which can now be used in the design of sensitive diagnostic systems for various types of radio-activity. Innovative application of powerful laser systems has produced intense, controllable sources of exotic particle radioactivity for nuclear investigations.

Several students have received their Ph.D. degree in experimental nuclear science for their work on basic nuclear research or R&D projects.

Table of Contents

Executive Summary 1

Table of Contents 2

I. Summary of Research 3

Personnel 4

II. Research Accomplishments 5

II.1. Spinodal Vaporization – a Spontaneous Decay Mode of Highly Excited Nuclei 5

II.2. A New Prompt Heavy-Ion Induced Fission Mode 14

II.3. The Role of the EOS in Statistical Decay of Highly Excited Nuclei 23

II.4. Prompt "Necklace" Fragmentation of the Dinuclear System in Dissipative Reactions 27

II. 5. Characterization of a Novel Plastic Scintillator for γ-Rays, Neutrons, and Charged Particles 38

II.6. A New Experimental Platform for Exotic Particle Beams at the OMEGA/EP Laser Facility 38

III. Publications

Book 39

III.1. Articles 39

III.2. Presentations/Lectures 40

III.3. Ph.D. Theses 41

Bibliography 42

I. Summary

During the outgoing grant period (2013-2016), the University of Rochester (UR) Nuclear Science Research Group has made significant progress in understanding nuclear reaction modes at low and intermediate bombarding energies. This development is due to our theoretical observations and experimental discoveries of several novel reaction phenomena. In addition, extensive R&D of new scintillator materials has led to enhanced radiation detection capabilities for the community.

On the theoretical side, we were able to show[1] that, above a certain critical excitation energy, nuclear systems become unstable against a novel prompt decay mode, "spinodal vaporization." This instability is specific to nuclei and other bound but open systems. At the critical excitation, such systems must spontaneously undergo an indefinite thermal expansion, accompanied by surface mass ejection into space. The process is faster than all decay modes previously known for excited nuclei and sets an upper limit for excitation energy and temperature of any equilibrated (compound) nucleus. The mechanism explains previously puzzling observations of limiting nuclear temperatures in heavy-ion reactions and holds the key for understanding the copious emission of nuclear clusters in such reactions. These studies also resulted in a set of statistical model parameterizations allowing to extend simulation calculations into the regime of nuclei excited to the limits of prompt instability.

On the experimental side, we can report[2] evidence for a prompt fission-like reaction mechanism following the transient fusion of ^{78}Kr and ^{40}Ca nuclei in central collisions at a relatively low bombarding energy of E/A =10 MeV. While linear momentum transfer to the intermediate composite is complete, the collective motion is not completely stopped before the mechanical stress disrupts the intermediate nuclear system again. The observation recalls the "L-window for fusion" phenomenon predicted already by early reaction theory[3] and reappears in modern density functional model calculations[4]. The effect is important, as it presents an independent measure of the nuclear equation of state, notably the tensile strength of finite nuclei. In spite of experimental efforts, it has previously not been demonstrated experimentally.

Yet another unexpected observation was made in the analysis of ^{48}Ca + ^{112}Sn and ^{48}Ca + ^{124}Sn collisions measured[5] at a bombarding energy of 45 A MeV. For the first time, several (at least 2) correlated nuclear clusters ($3 \leq Z_{IMF} \leq 7$) were demonstrated to be emitted in an aligned, quaternary fission-like process associated with multiple neck disintegration. This conclusion is deduced from analysis of individual reaction products and the kinematic relationships between reaction products. Preponderance of evidence for the unusual process is provided by the invariant cross section, relative velocities and angular distributions of cluster pairs relative to the projectile remnant.

Extensive in-beam tests of a new plastic scintillator (EJ 299-33) have established outstanding properties of this material, which are of practical significance. The scintillator provides not only n-gamma discrimination but exhibits radiation-specific response also to energetic charged particles ranging from isotopes of hydrogen to isotopes of carbon. Detailed investigations of the dependence of scintillator light output on particle species and energy are conducted in the framework of Birks theory[6,7].

The development of the experimental platform LIANS (Laser Induced Ion Acceleration for Nuclear Science) at the powerful UR Omega/EP laser facility encourages the group to embark on unique and novel studies of cluster structure and low-energy nuclear reactions between light nuclei, which are highly relevant for models of stellar evolution.

During the reporting period, three students have completed and defended their Ph.D. theses in experimental nuclear science. All of them have already found positions in industrial and academic R&D or as full-time faculty at a four-year technical college.

Personnel

Dr. W. Udo Schröder,	Professor of Chemistry and Physics, PI
Dr. J. Toke	(Senior Scientist., until 03/2015)
Eric Henry	Graduate Student/Research Associate
Sheth Nyibule	Graduate Student, Department of Physics, R.A.
Matthew Sharpe	Graduate Student, Department of Chemistry

II. Research Accomplishments

II.1 Spinodal Vaporization – a Spontaneous Decay Mode of Highly Excited Nuclei

J. Tõke and W. U. Schröder
Departments of Chemistry and Physics, University of Rochester, Rochester, NY 14627, USA

Abstract

A previously unknown, prompt decay mode of highly excited nuclear systems is described, which sets in at a critical excitation energy per nucleon. It is driven by an unbounded spinodal instability, unique to nuclei and other self-bound but open systems. The system undergoes spontaneously an indefinite thermal expansion leading to mass ejection and vaporization into the surrounding open space. The mode is faster than, and distinctly different from, all previously known nuclear decay modes. It sets a natural limit for the thermalization of nuclear excitation energy.

1. Introduction

Understanding the limits of thermodynamic stability of excited nuclear systems has been a focus of numerous theoretical and experimental studies[8–12] from the dawn of nuclear science. Theoretical studies have so far been overwhelmingly concentrated on instabilities in bulk nuclear matter kept under con- trolled conditions and, notably, at a fixed volume al- lowing under certain circumstances for an unphysical buildup of a gas of free nucleons in thermodynamical equilibrium with the liquid phase. The model calculations show that under such condition, owing to the Van der Waals - like equation of state for uniform matter, three kinds of domains exist in the space of control- ling variables for such matter. Firstly, there are domains where uniform nuclear systems would be stable. Then, there are domains where the uniform matter would be metastable and where, given time, it would end up as a two-phase system as a result of evaporation or condensation. And, finally, there is a domain commonly named spinodal, where uniform matter would be unstable and would spontaneously separate into liquid and gaseous phases. The above domains are readily identifiable, e.g., on the standard plots of Van der Waals' isotherms as functions of specific volume and pressure.

In contrast to the above theoretical view, experimental studies necessarily involve finite nuclear systems formed in the course of nuclear reactions. Such systems are not subject to external confinement and are thus at best metastable - free to evaporate particles into open space and to undergo shape fluctuations leading to fragmentation - the two basic statistical decay modes of metastable excited compound nuclei. It is worth noting here that this metastability is at the very crux of sound thermodynamical models of nuclear decay, such as Weisskopf's evaporation model[13] and various models of compound-nuclear fission, as well as various numerical implementations of these models[14–17]. The lack of external confinement has, however, one other unavoidable consequence which is thermal expansion. The paramount importance of the latter at elevated excitation energies has been largely overlooked in theoretical modeling of the equilibrium-statistical decay of excited nuclear systems - other than these reported in precursor conference proceedings[18] of the present study.

The present work is part of a continued effort[19–24] to construct an open microcanonical framework for understanding decay phenomena of highly excited metastable nuclear systems produced in the course of heavy-ion collisions and the limits of compound-nuclear metastability of such systems. It reveals the crucial and hitherto unappreciated role of thermal expansion in a peculiar *thermal* spinodal destabilization of highly excited nuclear systems. The latter gives rise to a hitherto unknown prompt decay mode of such systems, named here spin- odal vaporization, which then imposes a natural upper limit on excitation energy, a compound-nuclear system is capable of thermalizing and a limit on the domain of validity of the very concept of a compound nucleus. It is worth noting that while the existence of a limit on such validity has always been understood, beginning with the seminal work by Weisskopf[13], its actual location on the excitation energy scale has not been accurately specified.

The term ”open microcanonical” is used here to stress the fact that, unlike conventional microcanonical models of statistical nuclear decay, the formalism used here explicitly acknowledges lack of external confinement and thus allows for both, large-scale shape fluctuations and thermal expansion. Note, that the lack of external confinement translates into the pressure at the periphery of the system (microcanonical pressure) being zero regardless of the excitation energy or (microcanonical) temperature, which clearly is the case for excited atomic nuclei in vacuum.

$$a_{config} = \alpha_o \rho_o^{2/3} \int \rho(\vec{r})^{1/3} d\vec{r}, \qquad (2)$$

2. Theoretical Framework

The present study utilizes elements of a thermodynamic framework developed over many years of studies of the properties of highly excited nuclear systems, both, infinite and finite.[19–24] The model is based on the fundamental thermodynamical principle that an isolated system will assume macroscopic configurations fluctuating around the one that shows highest Boltzmann entropy, when- ever such exists. These maximum-entropy configurations are homogeneous for infinite systems and isotropic with a smooth density profile, for finite systems. As infinite systems one generally understands systems that are large enough to warrant neglect of the inhomogeneous surface domain. In contrast, the latter surface domain is of essence in modeling the behavior of finite systems. The above assumptions of uniformity and isotropicity are well justified given the nature of the formalism used. Naturally, for a self-bound object residing in vacuum, such as an excited atomic nucleus, maximum entropy is indicative of zero microcanonical pressure regardless of the excitation, as that pressure is given by the first derivative of entropy with respect to volume. For infinite systems, the pressure is then uniformly zero, while for finite system only the pressure at the periphery (microcanonical pressure) is zero, while in the interior bulk matter it is greater than zero as a result of the action of the surface tension. In the latter systems, the surface tension decreases with increasing excitation energy and so does the pressure of the bulk matter.

Boltzmann entropy is evaluated in the framework of zero-temperature Fermi gas model and Thomas Fermi approximation. The zero-temperature formalism was utilized for the sake of simplicity, but it is also a reasonably good approximation in the range of excitation energies considered. Thus, Boltzmann entropy is expressed as:

with E, a_{config}, and E_{config} denoting the total energy, the level density parameter, and the interaction energy of the configuration considered, respectively. The latter represents the zero-temperature energy of the configuration considered. It includes potential energy and the Pauli kinetic energy of the Fermi matter. Equation 1 is the base equation of the model, allowing one to evaluate S_{config} for any configuration of interest, characterized solely by the matter density distribution $\rho_{config}(\vec{r})$.

$$S_{config} = 2\sqrt{a_{config}(E - E_{config})}, \qquad (1)$$

The level density parameter a_{config} was calculated using the formalism proposed in Ref. [25]:
where α_o expresses the value of the level density parameter per nucleon at normal matter density ϱ_o.

The interaction energy is here calculated by folding a standard Skyrme-type EOS interaction energy density $\varepsilon_{\text{int}}^{EOS}(\rho)$ with a Gaussian folding function, and the folding length adjusted so as to approximately reproduce the experimental surface diffuseness of finite droplets of nuclear matter.

For the equation of state, the present study adopted a standard form consistent with Skyrme-type nucleon-nucleon interaction, which implies the interaction energy density (appearing in Eq. 3) in the form of

The values of the parameters a, b and σ in Eq. 4 are determined by the requirements for the binding energy, matter density, and the incompressibility modulus to have prescribed values. The values chosen in this study of a=-62.43 MeV, b=70.75MeV, and $\sigma = 2.0$ imply a normal density of $\varrho_o = 0.168\, fm^{-3}$, binding energy per nucleon at normal density of $\epsilon_{EOS}/\varrho_o = -16$MeV, the incompressibility modulus of $K = 220\ MeV$, and Fermi energy at normal density of E_{Fermi}=38.11 MeV.

One notes that in the model calculations for uniformly distributed matter, the finite range of interaction

$$E_{int}^{EOS} = R_{Gauss} \int \epsilon_{int}^{EOS}(\rho(\vec{r} - \vec{r}'))e^{-\frac{(\vec{r}-\vec{r}')^2}{2\lambda^2}} d\vec{r}d\vec{r}', \quad (3)$$

is of no consequence and the configuration energy can be written simply as $E_{config}=V\epsilon_{EOS}(\varrho)$, where V is the system volume. One notes also, that the results of the calculations do not depend critically on the actual parameterization of the equation of state and that a simple harmonic interaction results in similar overall trends

$$\epsilon_{int}^{EOS}(\rho) = \rho[a(\frac{\rho}{\rho_o}) + \frac{b}{\sigma + 1}(\frac{\rho}{\rho_o})^{\sigma}] \qquad (4)$$

as the one used in the present study.

At the crux of the present study lies a particular kind of spinodal instability unique to open microcanonical systems. In this respect, it is worth recalling that spinodal instabilities are always associated with certain extensive state variables of the system being pairwise fixed, with ratios of these extensive variables then representing derived intensive variables, such as the matter density ϱ, excitation energy per nucleon E/N, and iso-asymmetry per nucleon $(N - Z)/A^2$. The important difference between the "true" and derived intensive variables is that the former (such as temperature T, pressure p, chemical potentials for protons and neutrons μ_p and μ_n) are idealizations and are formally fixed throughout the system by *fiat* of the ensemble considered, while the latter are being fixed only on average, allowing for fluctuations of their values across the system up to allowing for coexistence of liquid and gaseous phases with different matter densities, excitation energies per nucleon, and iso-asymmetries per nucleon. The importance of the derived intensive variables stems from the fact that the equation of state refers to their local values and so do the characteristic state functions for uniform matter, proper for ensembles considered. For the matter to be stable for a particular kind of thermodynamic ensemble, the characteristic state function for this ensemble must be either a convex (Helmholtz free energy for canonical ensemble and Gibbs free energy for isothermal-isobaric ensemble for iso-asymmetric systems) or a concave (entropy for microcanonical ensemble) function of its de- rived intensive variables. In mathematical terms, this means that Hessian (curvature matrix) of this characteristic state function must be either positive definite or negative definite, respectively.

In view of the above, it is clear that the character of possible spinodal instability not only depends critically on the kind of thermodynamical ensemble considered, but is also unique to this kind, as different ensembles fix different sets of state variables. And so, in the classical canonical ensemble, fixed are (intensive variable) temperature *T*, and extensive variables of volume *V* and the number of particles *N*, allowing under circumstances for appearance of concavity of the Helmholtz free energy with respect to matter density and the resulting purely *mechanical* spinodal instability and ultimately liquid-gas coexistence. In contrast, in the classical microcanonical ensemble fixed are the extensive variables *V*, *N* and the total energy *E*, allowing this time under circumstances for convexity of entropy as a function of two derived intensive variables, ϱ and E/N. The corresponding Hessian is here a non-diagonal 2 by 2 matrix, with eigenvectors not aligned with either coordinate axis. Thus the possible spinodal instability will be of mixed *thermo-mechanical* character and will also ultimately result in coexistence of liquid and gaseous phases with different densities and excitation energies per nucleon. For the open microcanonical ensemble considered in the present study, entropy is a function of the one derived intensive variable of E/N only, and its Hessian degenerates into a single-element (1 by 1) matrix. Accordingly, the possible spinodal instability here is of purely *thermal* character. In this case, the instability does not, however, lead to phase coexistence even as it leads first to phase separation. This is so because the gaseous phase is not self-bound and will inevitably vaporize further into the surrounding vacuum, synonymous with a prompt spontaneous decay of the system considered.

For the sake of completeness, it is worth noting that spinodal instabilities are absent altogether in ensembles which are defined in terms of only one extensive state variable in addition to the requisite number of intensive variables. Such ensembles do not fix (on the average) any derived intensive variables. They include the grand canonical ensemble, with the sole extensive variable being volume *V* and intensive variables being chemical potential μ and temperature *T*, and the isothermal-isobaric ensemble for iso-neutral nuclear matter with the sole extensive variable being this time the number of particles, while intensive variables being temperature *T* and pressure *p*.

3. Results

The general behavior of uniform Fermi matter can be well understood from the appearance of isotherms in the familiar Van der Waals type plots. These are illustrated in Fig. 1 for the bulk model matter with Skyrme-type EOS with a compressibility constant of K=220 MeV. The isotherms were constructed using the microcanonical approach, with *T* and *p* representing microcanonical temperature and pressure, and are identical to those computed in a canonical approach, in virtue of ensemble equivalence for uniform matter. The isotherms feature prominently the familiar *mechanical* spinodal domains of negative compressibility characteristic for canonical ensemble (such as section BD of the dotted isotherm in Fig. 1) at constant temperature *T* and volume *V* and such ensemble only. Note, however, that for nuclear systems, canonical ensembles are of purely academic interest only, as they cannot be implemented practically. Importantly, the isotherms in Fig. 1 feature also, albeit less conspicuously, the crucial *thermal* spinodal domain of negative heat capacity for a realistic self-bound open microcanonical ensemble in vacuum, i.e., at zero pressure. This domain is bounded at point B on one side and point C on the other. Point B is by construction the one where the zero-pressure isobar is tangential to a particular isotherm at the minimum of the latter, the isotherm being the one defining the boiling-point temperature. In a canonical representation, this isotherm has been termed in recent past as “flashing point” isotherm[26]. Point C represents the excitation energy at which the system becomes unstable against uniform indefinite expansion and in that sense the spinodal domain BC is here open-ended. In this domain BC nuclear matter will undergo phase separation, with part of it condensing to- ward point B and the other part vaporizing toward point C and beyond, i.e., undergoing vaporization.

That the domain BC in Fig. 1 is indeed *thermal* spinodal is evident when one follows the evolution of a self- bound system at zero pressure (isobaric system) with increasing excitation energy per nucleon, starting at point A in Fig. 1 (normal density at zero excitation and zero external pressure) towards point B, and beyond. The excitation is measured here (for the correspondence be- tween the excitation energy and specific volume see Fig. 2) by the specific volume displayed on the abscissa and the trajectory of such an *isobaric at zero pressure* evolution is illustrated by the dashed line AC. One notes readily, that first, the temperature rises with increasing specific excitation energy, while the system undergoes thermal expansion. This rise in temperature is indicated by crossing of isotherms with progressively higher temperature indices as one proceeds from point A to point B. However, beginning at point B, the trend reverses and now isotherms are being crossed with progressively lower temperature indices, indicative of the heat capacity becoming formally negative. This indicates that at point B the system enters (*thermal*) spinodal domain of convexity of Boltzmann entropy as a function of excitation energy and, thus becomes unstable against phase separation. Not only can it not exist in this domain as uniform matter, neither can it exist here as a two-phase system. This is so, because the vapor phase is not self-bound and will expand indefinitely at the expense of its own energy content upon reaching spinodally (at the expense of energy derived from neighboring parts) point C in Fig. 1. Which means, that upon acquiring excitation energy in excess of what is needed to reach the "boiling" point B, the system will promptly shed a portion of itself via a boiling-like process named here spinodal vaporization, leaving behind a "leaner" metastable residue at point B. The latter will subsequently decay statistically via well-known decay modes of evaporation and fragmentation showing the source temperature as that at point B, regardless of the initially acquired excitation energy per nucleon. One may posit that the spinodal vaporization is akin to boil-

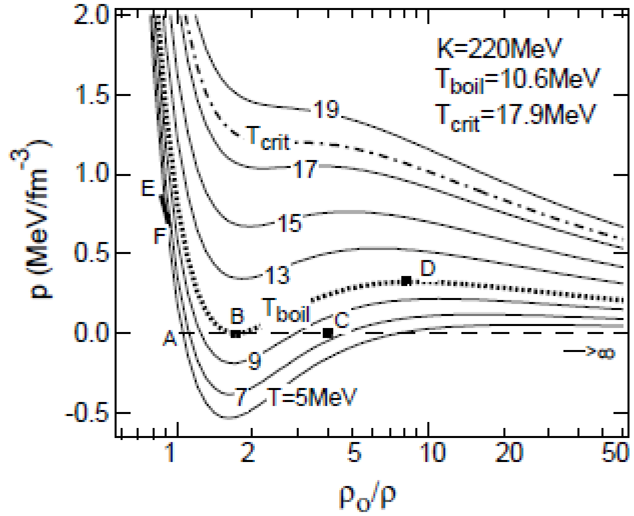

Figure 1: Isotherms for the model matter. The isotherm corresponding to zero-pressure boiling temperature is shown in dotted line and the critical isotherm is shown in dash-dotted line. The adiabatic trajectory for a hypothetical infinite system at zero pressure is shown in dashes (line AC), while such for the bulk of a finite (A=100) system is shown in bold solid line (line EF, see text). Point B represents both, the lower (low specific volume) limit of the *mechanical* (canonical ensemble) and the lower (low excitation energy) limit of the *thermal* (open microcanonical ensemble at zero pressure) spinodal domains, while points D and C represent the upper (high specific volume or high excitation energy) limits of these domains, respectively.

ing, even as in practical realizations the latter may to some extent rely on nucleation phenomena. The isotherm labeled as T_{boil} in Fig. 1 is by definition the one that is tangential to the zero-pressure line in its minimum.

The purpose of Fig. 1 is to demonstrate that any self- bound Van der Waals system (one that features characteristic Van der Waals isotherms) at zero pressure would enter the spinodal domain with necessity, and not by *fiat* of modeling, as soon as its initial energy is raised in excess of that at point B, and that the vaporization must take place regardless of whether any "conventional" statistical decay channels are open or not.

While Fig. 1 proves the inevitability of spinodal vaporization or boiling for any Van der Waals - like matter at elevated excitations and demonstrates that the phe-excitation energy per nucleon, starting at point A in Fig. 1 (normal density at zero excitation and zero external pressure) towards point B, and beyond. The excitation is measured here (for the correspondence be- tween the excitation energy and specific volume see Fig. 2) by the specific volume displayed on the abscissa and the trajectory of such an *isobaric at zero pressure* evolution is illustrated by the dashed line AC. One notes readily, that first, the temperature rises with increasing specific excitation energy, while the system undergoes thermal expansion. This rise in temperature is indicated by crossing of isotherms with progressively higher temperature indices as one proceeds from point A to point B. However, beginning at point B, the trend reverses and now isotherms are being crossed with progressively lower temperature indices, indicative of the heat capacity becoming formally negative. This indicates that at point B the system enters (*thermal*) spinodal domain of convexity of Boltzmann entropy as a function of excitation energy and, thus becomes unstable against phase separation. Not only can it not exist in this domain as uniform matter, neither can it exist here as a two-phase system. This is so, because the vapor phase is not self-bound and will expand indefinitely at the expense of its own energy content upon reaching spinodally (at the expense of energy derived from neighboring parts) point C in Fig. 1. Which means, that upon acquiring excitation energy in excess of what is needed to reach the "boiling" point B, the system will promptly shed a portion of itself via a boiling-like process named here spinodal vaporization, leaving behind a "leaner" metastable residue at point B. The latter will subsequently decay statistically via well-known decay modes of evaporation and fragmentation showing the source temperature as that at point B, regardless of the initially acquired excitation energy per nucleon. One may posit that the spinodal vaporization is akin to boiling, even as in practical realizations the latter may to some extent rely on nucleation phenomena. The isotherm labeled as T_{boil} in Fig. 1 is by definition the one that is tangential to the zero-pressure line in its minimum.

The purpose of Fig. 1 is to demonstrate that any self- bound Van der Waals system (one that features characteristic Van der Waals isotherms) at zero pressure would enter the spinodal domain with necessity, and not by *fiat* of modeling, as soon as its initial energy is raised in excess of that at point B, and that the vaporization must take place regardless of whether any "conventional" statistical decay channels are open or not.

While Fig. 1 proves the inevitability of spinodal vaporization or boiling for any Van der Waals - like matter at elevated excitations and demonstrates that the phenomenon in question has been in "plain sight" for all these years, a more conventional depiction of the instability is offered in Fig. 2 in the form of a caloric curve for the open-microcanonical system considered.

As seen in this figure, the caloric curve for such a system features prominently a domain of formal negative heat capacity, i.e., *thermal* spinodal instability. This domain ends formally at point C where the system becomes unstable with respect to uniform expansion, such that any portion of vapor reaching (spinodally) that point would expand further indefinitely. It is worth noting that the matter density behaves here monotonically with increasing excitation energy in the domain of interest, even as thermal expansion is here at the crux of the spin- odal instability. As pointed out earlier in Section 2, *thermal* spinodal instability is unique to open iso-neutral microcanonical systems, the only ones where the Boltzmann entropy depends solely on total energy per nucleon and the only ones where the convexity of entropy function translates directly into the formally negative heat capacity. In contrast, for iso-asymmetric systems spinodal instabilities in open microcanonical ensembles would be of mixed *thermo-chemical* character.

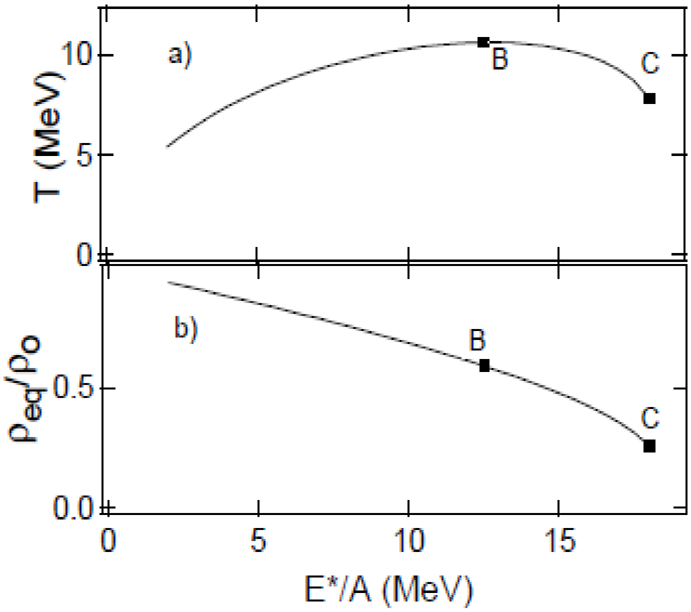

Figure 2: Caloric curve (panel a) and equilibrium density (panel b) as functions of excitation energy for a self-bound Fermi liquid under zero pressure. Points B and C correspond to those shown in Fig. 1.

The onset of spinodal vaporization is illustrated in Fig. 3 for a system of two equal masses in thermal contact. The present, purely open microcanonical picture allows for thermal expansion while keeping constant total excitation energy and mass number, but not the volume. As seen in this figure, at low and moderate excitation energies, maximum entropy occurs for a configuration where both (equal) parts have equal excitation energies, i.e., for uniform matter and excitation energy distributions. In this regime, the system may and will continually fluctuate away from uniformity, but the negative feedback of concave entropy will return the

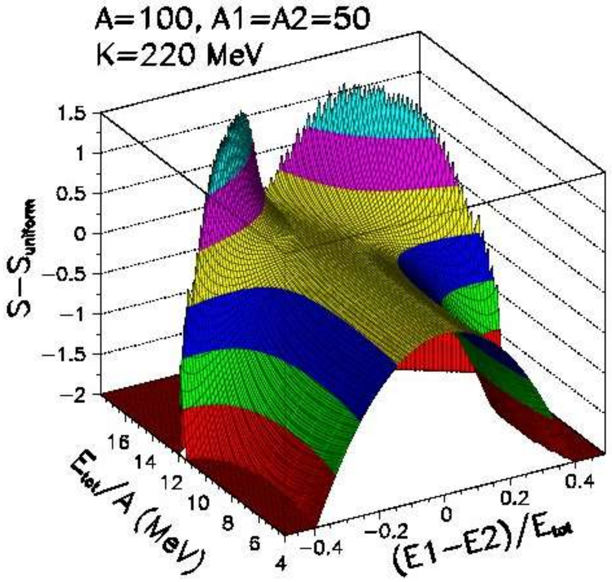

Figure 3: Reduced two-phase configuration entropy surface for a configuration of two equal-A subsystems with differing split of the available excitation energy E^* between the phases.

system back toward uniformity. The situation is dramatically different at excitation energies past the boiling point where the curvature of the entropy surface turns positive. From this point on, any randomly acquired asymmetry would be further reinforced by the action of entropy driving now the system further away from uniformity, with one portion eventually vaporizing away into the surrounding space. It is worth noting that in the spinodal domain of excitation energy, there is no hope of ever seeing the system at a state of approximate uniformity, even transiently.

For self-bound finite systems in vacuum, i.e., at zero external pressure, the presence of the surface domain alters the character of the possible spinodal instability in an important way. Here, the very term can no longer be associated with a matter configuration that is uniform in space, but rather with one that is solely isotropic around the center of the system and is describable in terms of a nonuniform density profile. For isoneutral matter considered in the present study, Boltzmann entropy is still a function solely of total excitation

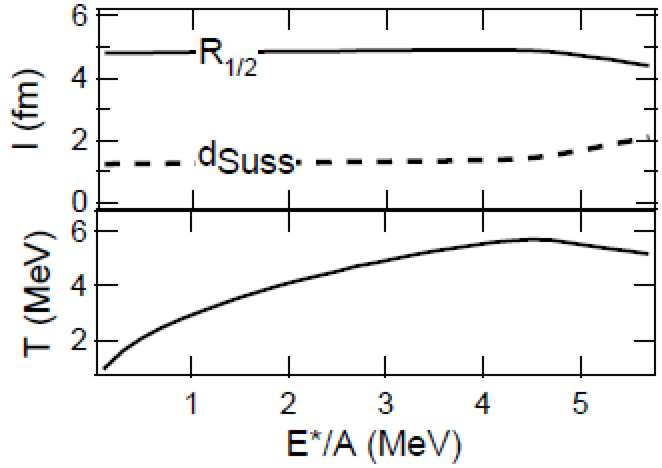

Figure 4: Evolution of the mass density distribution parameters and the microcanonical temperature with excitation energy per nucleon (See text).

energy, and the on- set of spinodal instability can be still inferred from the appearance of the system caloric curve.

The latter is illustrated in Fig. 4, along with the evolution of the two parameters, the half-density radius $R_{1/2}$ and the surface diffuseness (Süssmann width[27]) parameter *d*, that were used to parameterize the error-function like matter density profile[25]. As seen in this figure, the *thermal* spinodal instability sets now in at a significantly lower temperature than it did for bulk matter. This reflects the fact that the system has now an overall lower binding energy, but mostly the fact that the surface domain is more loosely bound than the bulk. One notes, that in the spinodal domain of a formally negative heat capacity, it is the surface domain alone that tends to expand with increasing energy, while the bulk tends actually to contract while staying at all energies safely outside of its own (*thermal*) spinodal instability domain (*vide* Fig. 2). This is indicative of yet another new type of spinodal instability, the one where sections of the system within one fraction of the solid angle increase first their surface diffuseness while harvesting energy from the neighboring sections that undergo contraction, and while cooling down in the process. Subsequently, surface domains in these fractions vaporize into the surrounding vacuum at the expense of their own energy content, all while keeping cooling down. This process is named here surface spinodal vaporization. The trajectory of the bulk (quasi-uniform) interior matter of the finite system considered here is mapped in Fig. 1) as a segment of line labeled EF reflecting reduction of the surface tension and, thus, the pressure in the interior with increasing (microcanonical) temperature. The pressure of the bulk matter is evaluated as microcanonical pressure at the density and the specific excitation energy of the (uniform) bulk matter. Note, that the latter pressure is of academic interest only and plays no role in why and how the *thermal* spinodal instability sets in. Here, it helps understand that the *sur- face* spinodal instability sets already in where the bulk interior matter alone is still stable.

4. Summary

In summary, the present study reveals the importance of thermal expansion for the fate of highly excited nu- clear systems. It reveals the unavoidability of eventually entering the *thermal* spinodal domain, when the excitation energy injected into the system is increased in excess of a certain critical energy per nucleon that can be naturally associated with the boiling-point temperature. The study reveals a new, hitherto overlooked, decay mode of highly excited nuclei consisting in indefinite expansion of fragments of the surface domain ending in their vaporization - a process named surface spinodal vaporization. For infinite matter (of academic interest only) the spinodal vaporization is a volume phenomenon entailing indefinite growth or vaporization of various portions of matter throughout the volume of the system. While one can freely speculate about what is really happening in the spinodal domain, the underlying thermodynamic theory is helpless in this respect. What the latter can do, however, is to tell with certainty that, when formally in spinodal domain, the system lacks metastability such that there is no local maximum in the entropy function. Hence, the system will promptly shed some parts of itself along with an unfairly large share of excitation energy via vaporization, before arriving at a state of compound-nuclear metastability. The latter is then subject to conventional nuclear thermodynamic modeling.

The present study has numerous experimental implications, with the existence of a limiting temperature being the most prominent of them. It so happens, that the experimental verification of the existence of a limiting temperature is there since very many years [2] and was, actually awaiting a plausible theoretical explanation. Further, the model calculations imply that the vaporized matter is colder than the residue, a prediction that may possibly find an experimental confirmation. They imply also an unusually low latent heat of vaporization that is measured on the excitation energy scale from the boiling point energy per nucleon to the point of the onset of instability with respect to uniform expansion - a mere few MeV per nucleon (cf Fig. 2). Furthermore, the nature of the model calculations is such that one can expect effects of the N-Z asymmetry, as previously reported[18].

II.2 A New Prompt Heavy-Ion Induced Fission Mode

E. Henry, S. Nyibule, M. J. Quinlan, H. Singh, J. Tõke and W. U. Schröder
Departments of Chemistry and Physics, University of Rochester, Rochester, NY 14627, USA

Abstract

Fission instabilities can be induced dynamically by the mechanical and thermal stresses to which intermediate systems produced in heavy-ion reactions are exposed. Such processes are poorly understood but should reveal independent evidence for the nuclear equation of state, notably the tensile strength of finite nuclei. This paper presents experimental evidence in support of a potentially new mode of prompt fission of the composite nucleus formed in central ^{78}Kr+^{40}Ca collisions at E/A=10 MeV, only a few MeV per nucleon above the interaction barrier. The new process bears semblance of the “L-window for fusion” predicted by early TDHF theories and potentially reappearing in modern DFT model calculations.

In addition, experimental data are discussed for the fission-like decay of projectile-like fragments from dissipative ^{48}Ca+^{112}Sn interactions at E/A=45 MeV occurring in proximity of their heavier reaction partners.

1. Introduction

Over the past three quarters of a century following the discovery[28–30] of nuclear fission, this process has been studied intensely for a range of medium-weight to heavy nuclei, mostly at low excitation energies and spins, using a variety of nuclear and electromagnetic probes[31,32]. Major research goals have been to explore the limits of nuclear stability and to map geometric pathways of fission, guided by expectations based on macroscopic liquid-drop[30,33–37] or rotating liquid drop models[38,39] (RLDM) for nuclear shapes and deformations. Mean-field symmetries for deformed nuclear shapes[40] have been shown[31,41–43] to have significant influences on nuclear stability and, specifically, on the geometry of the fission barrier, featuring one or more secondary wells and producing interesting and rich fission phenomenology.

Sustained experimental and theoretical research activities have led to a satisfactory conceptional understanding of fission occurring from an equilibrium, compound-nucleus state at low specific excitations, $E^*/A \lesssim 1$MeV. In many cases, theory has been able to make rather accurate quantitative predictions of fission probabilities, relative to competing decay channels, and of fission product distributions. However, it has so far proven very difficult to predict, within a comprehensive theoretical framework, the evolution of fission or fission-like modes observed for nuclei whose masses or mass-to-charge ratios are very different from those of the stable valley[44], or for those that receive significant transfers of momentum, energy, or spin within brief nuclear interactions. Yet, such fission-like modes have routinely been observed for systems produced in heavy-ion reactions at Fermi bombarding energies (E_{lab}/A = (20 – 100) MeV) and, occasionally, even below (see, e.g., Ref. [45–50]).

One of the well-documented examples of such processes is the emission of (one or several) massive clusters ("intermediate-mass fragments," IMF) in heavy-ion reactions, which resembles statistical fission-like decay of a nuclear system excited near the limits of its stability. However, while fission-like emission of multiple clusters from heavy systems has been considered and shown [Swi58] to be energetically possible already early in the discussion of nuclear fission and other decay mechanisms, later statistical models of so-called multifragmentation (cf. Ref.[51–53] and others) relied on simplifying, but highly disputable, *ad hoc* assumptions to fit just certain subsets of experimental data in terms of a postulated nuclear "liquid-gas phase transition." It is noteworthy that such methods are still sometimes used in theoretical studies (e.g., Ref.[54]) of fission barriers at finite nuclear temperatures.

Another type of essentially binary nuclear disintegration of projectile-like (PLF), target-like (TLF) or intermediate dinuclear system (DNS) in heavy-ion reactions is apparently dominated by dynamics. Reported examples are the snapping of the matter bridge ("neck") between nascent reaction fragments[55–57], a process akin to ternary fission[31,58,59], and the binary splitting of one or both of the main fragments following a dissipative reaction, occurring still within the range of substantial Coulomb and/or nuclear interactions[45,46,60–64] [SinQ11, Wilcz12].

While it is clear from the above that the field of nuclear fission research still has a range of questions to investigate, it is already possible to use fission phenomenology and quantitative systematics as diagnostic tools for investigating fusion and dissipation processes, as well as to probe the nuclear mean field "equation of state" (EOS), specifically the nuclear tensile strength and its transformation with isospin, excitation energy and spin. The following Section II provides some examples for the EOS related physics that can be addressed in heavy-ion induced fission studies. In Section III, surprising experimental observations of an apparently new dynamic (shock induced) fission process will be reported, which apparently does not proceed through the compound nucleus (CN) stage. Section IV discusses regularities observed for the isotopic distributions of fragments from splitting of PLF following a dissipative reaction. The final section offers a summary and outlook.

2. Theoretical Motivation: Heavy ion induced fission and the EOS

Interest in heavy-ion reactions, specifically fusion-fission, at bombarding energies safely above the interaction barrier derives from their potential to map ultimate stability limits of finite nuclei by varying their A/Z ratio, excitation energy and angular momentum. Presumably, this regime avoids specific nuclear structure effects that come into play at bombarding energies near or below the barrier[65,66]. In fusion-fission reactions above the barrier, the nuclear mean field, realized in terms of a density (ρ), spin (σ) and isospin (δ) dependent energy functional $\varepsilon(\rho,\sigma,\delta)$ is important, both in the entrance (fusion) and the exit (fission) channel. However, the latter process is not the exact inverse of the first, and the exit channel effective field may contain single-particle and/or collective excitation modes, depending on the internal damping of initial disturbances of the matter distribution. Therefore, models are sought that treat entrance and exit channels on the same footing and are able to follow the system trajectory, even if it does not proceed through a compound nucleus (CN) state, where most information on nuclear dynamics would disappear.

In simple approximation, the multi-dimensional entrance-channel mean field for two interacting nuclei (Z_1, A_1) and (Z_1, A_1) is modeled in terms of an effective potential energy $V(r,\ell)$ depending on the nuclear center separation distance r, relative angular momentum ℓ, and reduced mass μ. It is given by a sum of Coulomb, nuclear and centrifugal potentials, e.g.,

$$V(r,\ell) = \frac{e^2 Z_1 Z_2}{r} + V_N(r) + \frac{\hbar^2 \ell(\ell+1)}{2\mu r^2} \tag{1}$$

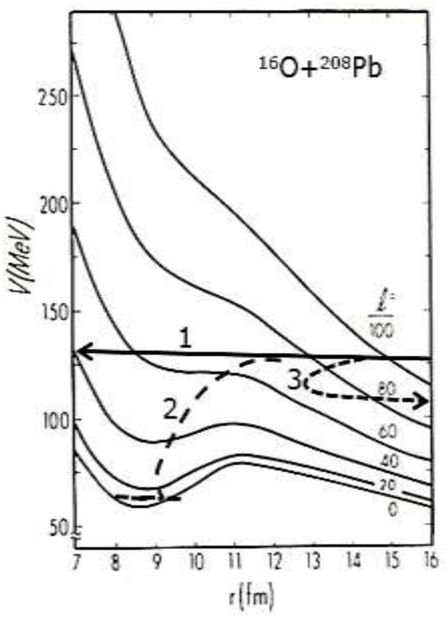

Figure 2: Radial dependence of effective $^{16}O+^{208}Pb$ interaction potential for different partial waves ℓ. Trajectory labels indicate elastic bounce-off (1), capture (2), and a dissipative reaction process (3).

As an example, the effective potential for $^{16}O+^{208}Pb$ is plotted in Fig. 1 vs. r and for various partial waves ℓ. Here, the nuclear potential V_N is taken as the proximity potential[67,68], which is based on the finite-range Gogny energy density functional[69]. Schematic trajectories in Fig. 1 are drawn to illustrate dynamic inhibition (Trajectories 1 and 3) of fusion in the $^{16}O+^{208}Pb$ entrance channel effected by compressional "bounce-off" (Trajectory 1) or deflection of the system trajectory away from the CN fusion path (Trajectory 3) by driving forces favoring mass or shape asymmetry[70], or by strong dissipation. Only one of those pictured (Trajectory 2) is trapped inside a potential "pocket," leading to capture and potentially to an equilibrated CN behind the unconditional saddle.

Modeling fusion for mass-asymmetric systems and bombarding energies above a well-defined barrier in $V(r,\ell)$, e.g., in terms of the proximity interaction model with one-body frictional forces[68,71], it is typically concluded that fusion should occur (Fig.1, Trajectory 2) from $\ell = 0$ up to a critical value $\ell = \ell_f$. This implies an approximately triangular cross section distribution $d\sigma_f/d\ell \propto \ell \cdot T_\ell(E) \cdot P_{CN}(\ell,E)$, where $T_\ell(E) \sim \Theta(\ell_g - \ell)$ is an entrance-channel transmission coefficient admitting all partial waves up to the grazing angular momentum ℓ_g. The probability $P_{CN}(\ell,E)$ defines the fusion range, i.e., the corresponding ℓ "window," $[0,\ell_f]$. It represents the probability for equilibration [SwiW05] of the dinuclear entrance channel shape and its relaxation into a CN. This leads to a *CN* fusion cross section of

$$\sigma_f(E) = \frac{\pi\hbar^2}{2\mu E}\left\{\sum_{\ell=0}^{\infty}(2\ell+1)\cdot T_\ell(E)\cdot P_{CN}(\ell,E)\right\} \tag{2}$$

The domain $\bar{P}_{CN}(\ell,E) = 1 - P_{CN}(\ell,E)$ corresponds to dissipative and quasi-fission reactions residing at the upper partial waves. The excited CN produced within the fusion ℓ window subsequently decays statistically via emission of light charged particles, producing evaporation residues (ER), or via fission and similar processes. The competition between these two decay processes is thought to be governed by the angular-momentum stability criteria of the Rotating Liquid Drop Model (RLDM) which has been developed[38] essentially for ground state nuclei. Application to heavy-ion reactions requires extrapolation of the model to hot nuclei, taking account of their expansion and surface destabilization, as discussed further below.

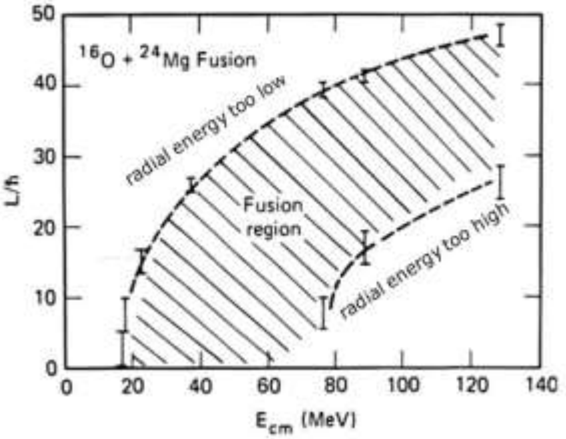

Figure 3: Theoretical (TDHF) prediction for the energy-L region in which complete fusion should occur (hatched) for the reaction $^{16}O+^{24}Mg$. After Ref [75].

Traditional analyses of fusion data assume a fusion probability of $P_{CN} \approx 1$, for a band of low ℓ waves, $\ell \geq 0$, i.e., central collisions, at above-barrier energies. This followed a period of unsuccessful search for the so-called "L-window for fusion" predicted by TDHF model calculations of the 1970s and 1980s [Ref. [3,72–75]] for energies of a few MeV per nucleon. An example of such (TDHF) predictions[75] is given in Fig. 2, where the range in the E_{cm} -ℓ plane is shown hatched where fusion is allowed. While the upper ℓ-wave boundary is immediately plausible, the one forbidden for the more central collisions is less direct to explain within the microscopic model. Here, insufficient nuclear stopping power allows projectile and target nuclei to pass through one another, emerging back to back at a 180^0 c.m. angle relatively unscathed.

Concerns as to the lower grade of computational efficiency, accuracy and completeness could be used to challenge the realism of the above early TDHF calculations. It is therefore significant and interesting that more recent, self-consistent time-dependent TDDF calculations[76,77] using density functional theory[78,79] predict a similar transparency effect in central fusion-type heavy-ion collisions. In Fig. 3, results of such calculations with Skyrme-type (SLy5) functionals are illustrated, showing three snapshots of the density contours of projectile- and target-like fragments in a central ($\ell = 0$) $^{78}Kr+^{40}Ca$ collision at E/A = 11 MeV, along with the fragment velocity directions. This is the actual system for which experimental results are discussed in Section III.

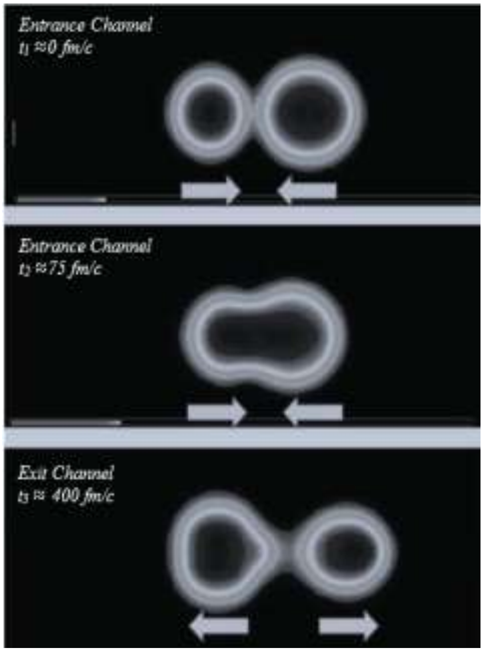

Figure 4: Density contours of projectile- and target-like fragments in central $^{78}Kr+^{40}Ca$ collisions at E/A = 11 MeV predicted by TDDF calculations[134]. Shown are snapshots for the indicated reaction times t_1-t_3.

The above calculations predict a prompt asymmetric fission mode to be established at times of the order of a few 100 fm/c after touching in the entrance channel. The corresponding period of this dynamic fission mode and the associated energy scale of (3-5) MeV are characteristic of single-particle motion but quite uncharacteristic of regular CN fission, which is a slow collective process. The few calculations that have already been performed with the TDDF model suggest the existence of an energy threshold for transparency, as well as sensitivity to the assumed EOS and to the entrance channel configuration of, possibly deformed, projectile and target nuclei.

In this context, related theoretical efforts should be pointed out, considering particular mechanisms for fusion inhibition at low energies and/or for heavy systems in terms of a deflection away from the fusion path by mass-asymmetric driving forces[70,80,81] or by diabatic repulsion[80–82]. Presumably, there are experimental observables such as fragment angular distributions and correlations that would allow one to distinguish experimentally between the various mechanisms.

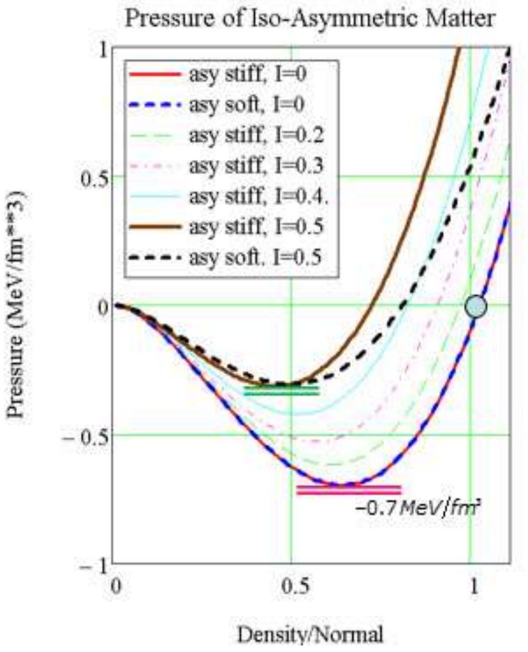

Figure 5: Thermal pressure P vs. matter density ρ/ρ₀, for different neutron excesses I=(N-Z)/A, based on a Skyrme-type nuclear EOS. The tensile strength is indicated by horizontal bars for I=0.

While there are yet few microscopic studies of the dependence of dynamic fission modes on mass-to-charge ratio (isospin), excitation and entrance-channel angular momentum, qualitative to semi-quantitative expectations can be formulated based on the available knowledge about the underlying nuclear EOS. A highly simplified EOS, based on Skyrme-type energy functionals, is illustrated in Fig. 4 for various neutron excesses *I*. It has the form

$$\varepsilon(\rho,I) := \varepsilon_0(\rho) + c_I \cdot I^2 \quad ; I := (N-Z)/A \tag{3}$$

with c_I a constant related to the symmetry energy and

$$\varepsilon_0(\rho) := \langle E/A\rangle \approx \underbrace{\langle E_{kin}/A\rangle}_{(3/5)\varepsilon_F}\left(\frac{\rho}{\rho_0}\right)^{2/3} + a\left(\frac{\rho}{\rho_0}\right) + b\left(\frac{\rho}{\rho_0}\right)^{5/3} \tag{4}$$

Here, ρ_0 is the saturation nuclear matter density, and the quantities ***a*** and ***b*** are constants. The associated nuclear tensile strength is defined as the minimum of the (negative) internal pressure, $P := \rho^2(\partial\varepsilon/\partial\rho) \leq 0$. It has been estimated[83] as $P_{\text{int}}^{\text{min}} \approx -0.7\ MeV/fm^3$ for symmetric matter (*N* = *Z*). Asymmetric matter, featuring an excess of like nucleons, *I* > 0, is less stable than symmetric matter, as illustrated in Fig. 4 for a large neutron excess range. Similarly, thermal excitation reduces the tensile strength providing less nuclear cohesion. Once the tensile strength is exceeded, e.g., by an internal pressure surge or by an external load on the nuclear surface, nuclear matter promptly loses cohesion and disintegrates. The former dynamic fission-like event could be induced by compression/rarefaction waves following collisional impact shock, as suggested by the TDDF calculations discussed above. The latter could arise from opposition of interaction and inertial forces. For cold, symmetric nuclear matter, such a dynamic fission-like splitting can be initiated in heavy-ion reactions already at low relative energies, say, (1-2) MeV above the barrier[83]. It would certainly be very interesting to find out experimentally, what the parameters are that describe the influence of the EOS on dynamical fission and its damping at substantial excitations.

A host of experimental studies of low-energy fission, reviewed at various stages[31,32,65,66], have demonstrated the predictive power of the RLDM[38], for the onset of nuclear shape instability, with increasing angular momentum *J*, and of Bohr's compound nucleus model for the competition between fission and particle decay modes. However, as soon as the excitation energy *E*/A* exceeds a few MeV per nucleon, these models appear to break down, and new fission-like instabilities appear. There is mounting evidence that these new modes, like multiple cluster emission, are associated with the dynamics and thermodynamics of nuclear expansion. In a series of studies of excited nuclei in vacuum, treated[84,85] in the appropriate open micro-canonical statistical ensemble, it was noticed that, because of its high local level density, the nuclear surface plays an important role in this thermal expansion. The fact, that an excited dinuclear "daughter" system has much more surface and associated surface entropy than an excited “parent” mono-nucleus of the same A, Z and total energy, is cause for a very fast, “prompt” split of the parent nucleus.

The physical reasons for such behavior are understood from the fundamental proposition of the microcanonical statistical approach: Given a total excitation energy, E^*_{tot}, the nucleus expands to assume a new equilibrium density profile ρ_{eq}, cooling in the process and ending at maximum entropy *S*,

$$\left(\frac{\partial S}{\partial \rho}\right)_{E^*_{tot}} = 0 \quad \rightarrow \quad \begin{cases} \rho_{eq} \\ T \end{cases} \quad \begin{pmatrix} microcanonical \\ model \end{pmatrix} \tag{5}$$

Here, the microcanonical temperature *T* is defined via the density of states. Entropy *S* and thermal part, E^*_{th}, of the nuclear excitation energy are approximately related by

$$S = 2\sqrt{a \cdot E^*_{th}} \quad \text{with} \quad E^*_{th} = E^*_{tot} - E^*_{conf} \tag{6}$$

with a representing the nuclear level density parameter (“little *a*”). The latter has volume and surface parts[25],

$$a = a_{Volume} + a_{Surface} = (\alpha_V A + \alpha_S A^{2/3})(\rho/\rho_0)^{-2/3} \tag{7}$$

with a surface coefficient α_s about 3 times as large as the volume coefficient α_V. In Equ. (6), the thermal (kinetic) part of the total excitation energy of nucleus *A* is given by subtracting from the total excitation E^*_{tot} the configurational part, E^*_{conf}, which contains energy differences relative to the ground state such as due to expanded volume, shape differences and finite angular momentum $J \neq 0$. Obviously, the nuclear EOS enters the calculation of E^*_{conf}, in a significant fashion, because dilution of the matter density away from saturation consumes excitation energy.

The main effect of the expansion degree of freedom on nuclear fissility for excitations of more than a few MeV per nucleon stems from the softening of the nuclear surface region and the disappearance of the surface tension, which is quite dramatic[85] above $E^*/A \geq 4.5\ MeV$. This effect implies a reduction of the critical angular momentum where, according to the RLDM, nuclear droplet shapes become unstable, and a disappearance of binary fission altogether already at moderately high excitations. Better mapping of the fission domain would benefit the development of a RLDM for hot nuclei.

3. Experiments

Fission processes induced in several heavy-ion reactions at low (^{78,86}Kr+^{40,48}Ca at E_{lab}/A=10 MeV/A) and intermediate (^{40,48}Ca+^{112,124}Sn at E_{lab}/A=45 MeV/A) energies have been studied by the University of Rochester group[86,87] with the CECIL and ISODEC collaborations. Object in the inverse-kinematics reaction ^{78}Kr+^{40}Ca at E_{lab}/A=10 MeV/A was to search at forward angles for dynamical fission-like or splitting events. For orientation, the RLDM predicts loss of stability for the medium-weight composite systems (A_{tot}=118,

Z_{tot}=56) and (A_{tot}=172, Z_{tot}=70) against distortions from spherical shape for angular momenta above $J\approx 60$ ($\hbar$) and $J\approx 82$ ($\hbar$), respectively.

In the experiments, pulsed beams produced by the LNS Catania K600 cyclotron were used to bombard self-supporting calcium and tin targets of appropriate thicknesses (*1*-several mg/cm^2). Charged products were detected with the 1192 Si-CsI(*Tl*) telescopes of the CHIMERA 4π multi-detector array[88]. The data acquisition system provided ΔE/E energy, time-of-flight ($\Delta t\sim 1ns$) and pulse shape information, the latter only for a subset of Si detectors.

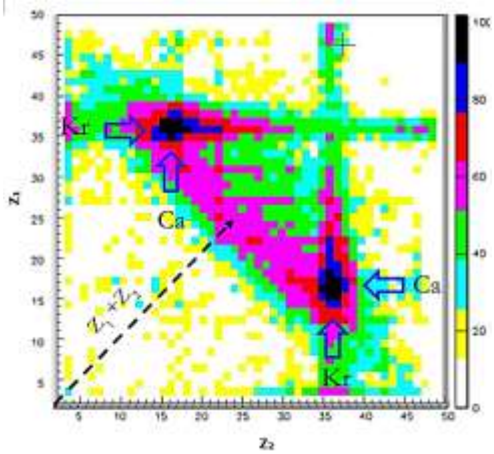

Figure 6: Typical charge correlations Z_1 vs. Z_2 measured at $\theta=5^0$ for the ^{78}Kr+^{40}Ca reaction at 10 A MeV. Plotted is the log of $d^2\sigma/dZ_1Z_2$. Arrows and labels identify projectile and target nuclei.

Figure 5 displays an experimental correlation between the atomic numbers of two detected fragments ($Z_i > 3$) on a log scale. Narrow distributions peaked near $Z_i\approx 36$ and $Z_i\approx 20$, clearly visible in the diagram, are attributed to projectile-like and target-like fragments, respectively, from dissipative collisions.

Of interest to the following are the events in the cross section ridge at $Z_1+Z_2\approx 48\pm 2$, adding up to 85% of the total charge of the system ($Z_{tot}=56$). However, the sum charge is shared between the two correlated fragments in terms of a very broad distribution peaking at symmetric splits. Corresponding mass correlations are also obtained for the same events, with $A_1+A_2\approx 106\pm 16$. Similar to the appearance of the Z_{tot} distribution in Fig. 5, the distribution of the sum of the masses of correlated fragments is also much narrower than the distribution in mass splits.

The evidence discussed above already strongly suggests a fusion-fission process as origin of the correlated fragments. This conclusion is strongly supported by all remaining fusion-fission type observables. For example, the measured folding-angle distribution of velocity vectors $\vec{v}_1^L$, $\vec{v}_2^L$ of the correlated fragments (1 and 2) indicates collinear, back-to-back emission of the fragments in the c.m. system. These velocity vectors and corresponding momenta are used to determine velocity components, parallel and perpendicular to the beam, in the rest frame of the emitter, the fissioning source.

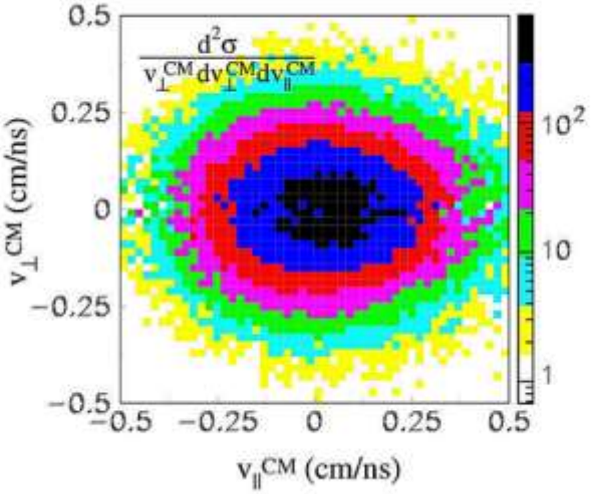

Figure 6: Correlated fragment velocities, parallel and perpendicular to the beam, in the rest frame of the emitter. Fragment with relative velocities in the gate defined in Fig. 8 are included. The velocity of the cm system in the lab has been subtracted.

The resulting invariant velocity plot is given in Fig. 6 for fragments with fission-like relative velocities. The origin of this plot has been taken as the velocity $\vec{V}_{cms}$ of the c.m. system in the lab. From the fact that this experimental velocity plot is centered at the origin, one concludes that the correlated fragments come indeed from the composite nucleus, which is at rest in the overall c.m. system and contains the entire system mass and linear momentum. A slight deformation of the distribution in beam direction is not seen in the spectrum of transversal relative velocities.

The spectrum of relative fragment velocities $v_{rel} = \left|\vec{v}_2^L - \vec{v}_1^L\right|$ is given in Fig. 7. It is bimodal, showing one peak centered at $v_{rel} = 4.5$ *cm/ns* which is attributed to the dissipative reaction component, whose presence is also expected for the system. Of particular interest in the present context is the second component peaking at the much lower velocity of $v_{rel} = 2.4$ *cm/ns*, slightly larger than is characteristic of equilibrium fission. The vertical bars in Fig. 7 indicate the velocity range accepted in the definition of fission-like events included in the velocity plot shown in Fig. 6. There is, obviously, a small contamination of this velocity domain by the tail of a component due to dissipative collisions.

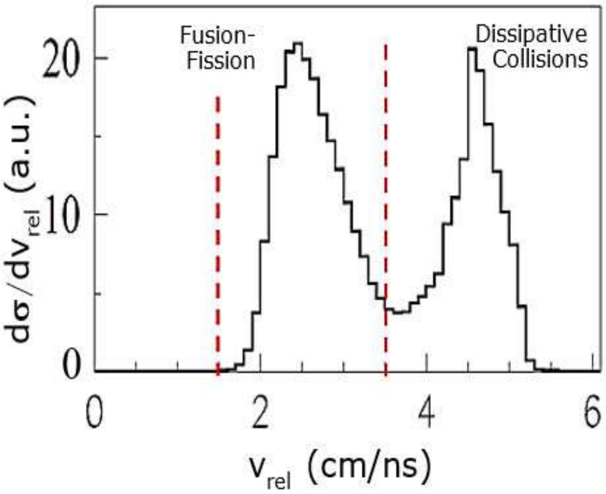

Figure 7: Distribution of relative velocities of correlated events in the reaction ^{78}Kr+^{40}Ca at E/A=10MeV. A collinearity condition of -1.0< cos(α)< -0.7 (see Fig. 8) was imposed on the fragments.

Therefore, for all intent and purposes, the correlated fragments described above come from a fusion-fission-like process. Its somewhat unusual properties include the shape of the fragment angular distributions $d\sigma/d\theta$, which is strongly anisotropic and, except for mass-symmetric events, not symmetric about 90^0. For asymmetric fission events, the heavier of the fragments is emitted preferentially forward in the c.m. system.

The experimental fission angular distribution of the heavy fragment, $d\sigma/d\theta_{HFr}$, is plotted in Fig. 8. Different symbols represent the indicated different ranges in fission fragment mass asymmetry defined as $\eta_A = (A - A_2)/(A + A_2)$. For symmetric events, $|\eta_A| < 0.1$, the distribution is symmetric about Θ_{HFr}=90^0, as it must be. But it is not isotropic and has maxima both at forward and backward angles. This behavior indicates a rather strong alignment of the fission axis in beam direction and demonstrates the dominantly dynamic character of the process. A weak contribution from regular CN fission to the ensemble of considered events is not excluded; its contribution can be estimated from the cross section around 90^0.

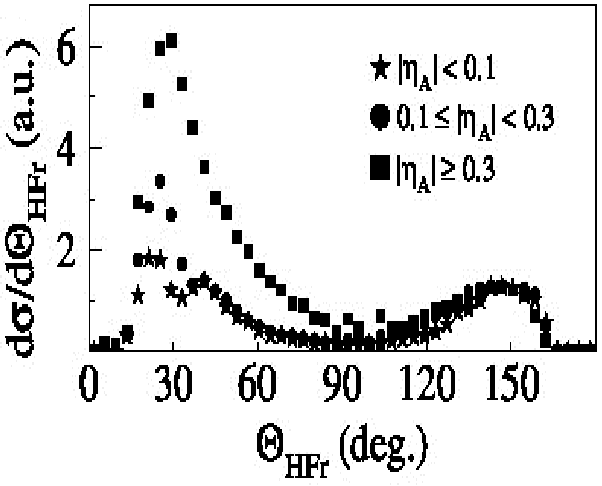

Figure 8*:* Angular distributions of the larger (of two) fragments in the center-of-mass system for three bins in mass asymmetry η_A , normalized to yields at backward angles.

Fragments are emitted in the process with significant excitation, as can be detected by their sequential evaporation of particles. In the experiment, sequential emission of alpha particles from the excited fission fragments was identified by the characteristic Galilei-invariant α-particle velocity distributions plotted with respect to the corresponding fragment emission direction. The scatter plot velocity distribution shown in Fig. 9 is a composite of events in which α particles from the forward going fragment populate the half plane $v_{\parallel}^{\alpha} > 0$, and those from the backward going fragment are plotted in the region $v_{\parallel}^{\alpha} < 0$. The resulting good matching of the two semi-circular velocity patterns demonstrates the correctness of identification of the emitters, as well as the quality of experimental calibrations.

As is already evident from the approximately constant invariant α particle cross section in Fig. 9, the spin angular momenta of the emitting fragments is negligibly small. This conclusion was shown to apply consistently to events emitted in good alignment of their fission axis with the beam direction, regardless of mass asymmetry. In contrast, fragments emitted into lateral directions (in the c.m. system) are associated with anisotropic a particle angular distributions, indicating significant intrinsic spin values J, as expected for equilibrium statistical fission.

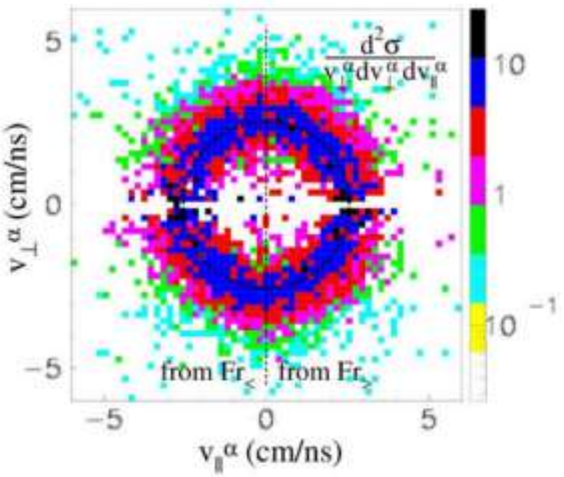

Figure 9: Galilei-invariant velocity distributions of a particles emitted from correlated mass-symmetric fission fragments. The parallel and perpendicular components are defined relative to the fragment velocity vectors.

4. Conclusions

Evidence has been presented for a dynamical fission-like process in which the composite system formed in central collisions with total mass, charge and linear momentum bypasses the compound nuclear equilibrium, at least partially, undergoes an essentially binary split into a broad mass and charge distribution. Strong memory of the beam direction is retained in a strongly aligned scission axis, with heavier fragments in asymmetric splits are preferentially emitted in the direction of flight of the projectile. The process is reminiscent of events predicted in microscopic theoretical calculations. The inability of the system to completely stop the relative motion appears to set limits on the tensile strength of the underlying nuclear equation of state.

Acknowledgements

The authors acknowledge the important contributions by their colleagues, members of the international ISODEC collaborations. Thanks are due Drs. V.E. Oberacker and S. Umar for providing results of their TDDF calculations prior to publication.

This work was supported by U.S. DOE Grant No. DE-FG02-88ER4014.

II.3 The Role of the EOS in Statistical Decay of Highly Excited Nuclei

J. Tõke and W. U. Schröder
Departments of Chemistry and Physics, University of Rochester, Rochester, NY 14627, USA

Abstract:
Application of *open* microcanonical ensemble theory developed by the group modifies previous concepts of statistical decay of highly excited nuclei at subnormal matter densities. Appropriately modified statistical decay codes can be used to describe and analyze compound-nucleus decay even approaching the boiling/vaporization domains. Such modified codes provide new tools for testing EOS and compound-nucleus concepts.

Isolated, moderately excited nuclei are metastable. They decay by slowly evaporating particles into the vacuum or undergo fission, which are the two basic statistical decay modes of compound nuclei, apart from γ decay in their final stages. Concepts of metastability constitute the base of sound nuclear thermodynamics[13]; they have spawned successful numerical implementations of nuclear decay[14–16].

For finite nuclei, expansion is governed by maximum Boltzmann entropy, which we relate to density (ρ) and shape dependent configuration energy $E_{config}\left[\rho(\vec{r})\right]$, as well as to the level density parameter $a_{config}\left[\rho(\vec{r})\right]$. For simplicity, the framework of a zero-temperature Fermi gas and the Thomas Fermi models are used, reasonable assumptions for excitation energies E^* much smaller than the mean Fermi kinetic energy, $E^*/A \ll \langle T_F \rangle \approx 20\,MeV$. Then, the above Boltzmann entropy can be written, as before,

$$S_{config} = 2\cdot\sqrt{a_{config}\left(E^* - E_{config}\right)} = 2\cdot\sqrt{a_{config}E^*_{therm}} \tag{1}$$

The configuration energy includes potential energy, Pauli kinetic energy of fermion matter, rotational energy, etc. Equ. 1 is the base equation of our model, allowing one to evaluate $S_{config}\left[\rho(\vec{r})\right]$ and level density parameter[25] $a_{config}\left[\rho\right]$ for any configuration of interest characterized by the equilibrium matter density distribution $\rho(\vec{r})$ which, in turn, depends on the underlying (iso-) EOS. A typical Skyrme-type EOS of the form

$$\varepsilon^0_{\mathrm{int}}(\rho) = \rho\left[a\cdot(\rho/\rho_0) + \frac{b}{\sigma+1}\cdot(\rho/\rho_0)^\sigma\right] + c_I(\rho/\rho_o)I^2 \tag{2}$$

is used in the present calculations, where $I = (N-Z)/2A$ is the isospin asymmetry parameter. Parameter values adopted in calculations are a = -62.43MeV, b = 70.75 MeV, σ = 2. They correspond to a saturation density of ρ_0=0.168 fm^{-3}, a normal binding energy of $\varepsilon^{EOS}_{\mathrm{int}}/\rho_0 = -16\,MeV$, a Fermi kinetic energy of $T_F = 38.11\,MeV$, and a compressibility modulus of K = 220 MeV. Using this EOS, one generates an associated finite-range version by folding with a Gaussian,

$$E^{EOS}_{\mathrm{int}} = R_{Gauss}\cdot\int\varepsilon^{EOS}_{\mathrm{int}}\left[\rho(\vec{r}-\vec{r}')\right]\cdot\exp\left\{-(\vec{r}-\vec{r}')^2/2\lambda^2\right\}d^3\vec{r}\,d^3\vec{r}' \tag{3}$$

The appropriate folding width (parameter λ ≈ 2 fm) is found by fitting experimental matter radii and the diffuseness of ground-state nuclei. For finite nuclei, expansion dynamics and relation to the underlying EOS are significantly affected by the structure of the nuclear surface.

The abbreviated discussion of thermodynamic stability and disintegration phenomena given above implies that our theoretical model should describe the state of the metastable compound nucleus up to the boiling point, i.e., it should predict conditions and specifics for compound-nuclear decay. This is of interest because such decay processes are amenable to experimental observation, and because our model provides a plausible and robust relation between decay phenomena and EOS available for meaningful testing and interpretation of observations. Since, however, no statistical code yet exists describing on a consistent footing the many decay modes observed [Col00] for hot, expanded nuclear systems in the domain of limiting temperatures [Nat02], we intend to embark on providing statistical model parameters capturing the essential physics described in open microcanonical theory.

The main physics contained in existing statistical model codes is encoded in the model level densities, their dependencies on nuclear excitation energy and spin, as well as the ground-state inertias, emission barriers, and Q-values. Decay probabilities are then calculated from a comparison of the entropies associated with competing decay channels [Wei37]. Most of the corresponding properties, safe for the fission barriers, for hot and expanded nuclei are quantitatively predicted by our model. Since the corresponding modifications to nuclear decay phenomena are a direct consequence of the underlying EOS, we propose here for the grant period,

1) to provide a scheme for upgrading the basic physics contained in conventional statistical codes for nuclear decay, and

2) to analyze existing data and/or conduct specific experiments testing the excitation function for emission rates and branching ratios predicted by such an upgraded statistical code.

The central equation of our theoretical model relates the maximized nuclear entropy S to the "little-a" level density parameter and the available thermal part (E^*_{therm}) of the total nuclear excitation energy (E^*_{tot}), as given by Equ. 1. The latter also contains collective deformation, compression and rotational energies as a combined "configuration energy" reducing the thermal excitation. In this fashion, the entropy is directly related to the EOS.

$$\left(\frac{\partial S}{\partial \rho}\right)_{E^*_{tot}} = 0;\ \left(\delta^2 S\right) < 0 \ \rightarrow \begin{cases} \rho_{eq} \\ T \end{cases} \left[EOS\right] \qquad (4)$$

The task is then to maximize the nuclear entropy for a given total excitation to obtain a metastable state. The level density parameter has volume and surface parts, with ground-state values fixed by experimental systematics[25]. As the nucleus expands, diluting the spatial matter density, the density of quantal energy levels of the Fermi gas increases according to the well-known power law,

$$a(\rho) = a_0 \cdot \left(\rho/\rho_0\right)^{-2/3} \qquad (5)$$

In its simplest (harmonic-interaction Fermi gas, HIFG) version of our model, the energy per nucleon depends quadratically on the matter density, with a curvature given by the incompressibility modulus K. In this approximation, the important quantities can be evaluated analytically. Closed-form relations have been developed for several of the most relevant decay model parameters, which can now be used to start modifying existing statistical computer codes such as CASCADE[15], PACE[16], GEMINI[89] and others.

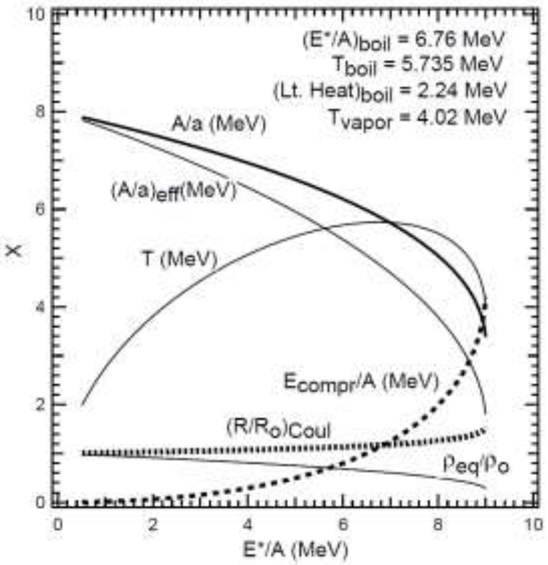

Figure 1: Statistical properties of a compound nucleus after equilibrium expansion to maximum entropy. Various quantities are plotted vs. total excitation energy per nucleon. E_{compr} denotes the non-thermal part of the total excitation energy, T the nuclear temperature, R the Coulomb radius, κ=A/a is the level density scaling factor.

Figure 1 displays model predictions for the dependence of several decay model parameters on the total excitation energy per nucleon (sum of thermal and configuration energies). The results were obtained for an EOS corresponding to a mean ground-state binding energy per nucleon of $E_{bind} = 8$ MeV and an incompressibility modulus of K = 220 MeV. Shown in the figure are the excitation energy dependence of the equilibrium density (curve labeled ϱ_{eq}/ϱ_o) of an expanded nucleus relative to the normal saturation density.

The quantity T represents the thermal energy per nucleon after expansion to equilibrium density, i.e., the microcanonical temperature. It is seen to increase to its maximum, the limiting temperature of $T_{boil} = 5.7\ MeV$, corresponding to an excitation of E*/A ≈ 6.8 MeV. At about $E^*/A = 9 \cdot E_{bind}/8$ The mean temperature of the nucleon vapor emitted from a boiling nucleus is calculated as $T_{vapor} \approx 4$ MeV, significant colder than the residue at boiling, a specific prediction for nuclear decay in vacuum.

One also predicts an increase in the Coulomb radius R_0 by up to 50%, leading to a significant reduction in the barrier for charged-particle emission and corresponding changes in spectrum shapes. Vertical slopes shown by the curves for several variables at about E*/A = *9* MeV indicate inherent system instabilities, which lead to sudden, non-statistical disintegration. Such, potentially mixed-mode instabilities have been treated in our more sophisticated, finite-range calculations conducted in past grant periods[1,23,90].

It is a significant advantage of our model description of highly excited compound nuclei that it builds upon the traditional description in terms of an interacting-Fermi gas model for the nucleus but logically extrapolates to higher excitations the very concepts incorporated in all statistical models codes such as CASCADE[15], PACE[16], GEMINI[89] and others. Hence, our model parameters represent extrapolations of previously constant parameters already contained in the traditional models. The envisioned modifications should account for several physical effects:

1) "Expansion cooling" of a hot nucleus at initially saturation density occurs because chaotic internal kinetic energy of nucleons is transferred to increase potential energy associated with the nuclear binding energy represented by the nuclear EOS.
2) Increased density of levels available to the expanded nucleus relative to those for saturation density, resulting from a lower matter density.
3) Decreased Coulomb energy barriers compared to ground-state nuclei because of expansion.

These effects change the branching ratios of competing decay channels, as well as the kinetic-energy spectra of the emitted particles but preserve the overall binding energies and decay Q-values. What needs to be explored quantitatively is the sensitivity of the branching ratios to the underlying EOS. The large increase with excitation energy E^*/A of the density of available levels is indicated in Fig. 7 by the relation κ=A/a, which starts from the ground-state value of κ=8 MeV to decrease by more than a factor of two. These quantities can have a large effect on decay probabilities and branching ratios, as they enter exponentially the statistical-model expressions for decay widths given by

$$\Gamma\left(E^{*}_{therm},J\right)\propto\varpi\left(E^{*}_{therm},J\right)\approx\frac{1}{24(4a)^{1/4}(\Im\mathrm{T}/\hbar^{2})^{3/2}}\frac{\left(2J+1\right)}{(E^{*}_{therm})^{5/4}}\exp\left\{2\left(a\cdot E^{*}_{therm}\right)^{1/2}-\frac{\left(J+1/2\right)^{2}}{2\Im\mathrm{T}/\hbar^{2}}\right\} \tag{6}$$

for a nucleus at thermal excitation energy E^{*}_{th}, temperature T, and spin J, where $\Im$ is a relevant effective moment of inertia. The quantity $\sigma^{2}=\Im\mathrm{T}/\hbar^{2}$ is the "spin cutoff" parameter describing the fall-off of the probability distribution for large spin angular momenta carried by an equilibrated nucleus. It depends on the macroscopic size and shape of the excited nucleus.

To explore the effect of nuclear expansion on the first (entropy) term $S=2\sqrt{a\cdot E^{*}_{th}}$ in the exponential in Equ. 6, one may consider the excess entropy $\Delta S=2a_{eff}(E^{*})\cdot T_{equ}(E^{*})-2\left(a_{0}\cdot E^{*}_{th}\right)^{1/2}$. This gain in entropy is a non-monotonic function of excitation. For an A=200 nucleus, it takes on large values between excitation energies of E*/A = 4 and 6 MeV. Here, one expects a decay branching that is rather different from that expected for the not expanded nucleus and, therefore, a sensitivity of branching to the underlying EOS. Note that the boiling energy is approximately E*/A=6.8 MeV, such that at such excitations, saturation-density nuclear matter does not exist in a meta-stable form. However, based on our general understanding of the thermodynamics of the decay of finite nuclei, we expect a relatively weak dependence of branching ratios on excitation energy slightly past E*/A ≈ 5.5 MeV.

It is tempting to speculate that, as additional energy is deposited in a nucleus, corresponding massive ejection of matter occurs from the surface region, surrounding an ever-decreasing nuclear bulk. Since the relative thermal velocities of nucleons in the separating patches of matter are still small, these domains can coalesce and form clusters. Certainly, the Rochester work on establishing a thermodynamic description of finite nuclei in an open micro-canonical approach has provided a pathway for achieving a final resolution of the long-standing puzzle of nuclear multi-fragmentation that continues to vex modern nuclear reaction theory.

II.4. Prompt "Necklace" Fragmentation of the Dinuclear System in Dissipative Reactions

S. O. Nyibule, M. J. Quinlan, E. Henry, H. Singh, J. Tõke and W. U. Schröder
Departments of Chemistry and Physics, University of Rochester, Rochester, NY 14627, USA

For the US-Italian CECIL Collaboration

Abstract:
Prompt, collinear emissions have been observed for 1, 2, and, possibly, 3 light nuclear clusters, trailing at mid-velocities the fast projectile remnants from mid-peripheral ^{48}Ca+^{112,124}Sn collisions at E/A = 45 MeV. Experimental evidence suggests that the chain of aligned light clusters (Z_{cl} = 3-5) is produced in the decay of massive, neck-like structures joining projectile-like and target-like fragments in transient dinuclear systems. The dynamical mechanism resembles ternary, quaternary and higher-multiplicity fission modes. It represents a tool for studying the tensile strength and dynamical instability modes of warm, viscous nuclear matter.

II.4. 1 Introduction

Since its beginnings, nuclear science has focused on the macroscopic shapes of atomic nuclei, droplets of a (Fermi) fluid *sui generis*. In spite of the enormous progress in understanding made in the past 75 years, explorations of the characteristic dependencies of the stable nuclear shapes and nuclear disintegration modes, on mass number A, neutron excess $I = (N-Z)/A$, excitation energy E^* and spin angular momentum J, are incomplete and need to continue[91,92]. As expected from macroscopic energetics[38,93], the most stable nuclei assume compact spherical, or nearly spherical, ground-state shapes that minimize nuclear surface energy. However, intrinsic quantal structure imposes strong deformations on nuclei in certain domains of the Segrè Chart[94]. In turn, internal structure may also constrain[95] nuclear shapes from becoming too compact, lending itself to observation and detailed theoretical evaluation[96–98]. Studies of the fine structure of the fission barrier[31,32,41,99], the shape of fission pathways[43] and explorations of the multi-dimensional potential energy landscapes in heavy-ion reactions[47], e.g., for the production of super-heavy nuclei[100,101] illustrate past utility of the connection between macroscopic shape dynamics and intrinsic nuclear structure for progress in nuclear science.

Spontaneous nuclear fission[31,32] and low-energy, fission-like dissipative heavy-ion reactions[47,102] are cases in point. These are essentially binary processes with only two ($M_F = 2$) massive primary fragments in the exit channel, even though Q-values would allow[103] simultaneous emission of multiple massive fragments. Because of intrinsic excitations acquired in the process, the hot primary reaction products de-excite in statistical decay. The latter fragments sequentially de-excite statistically, but on significantly longer time scales. Promptly emitted additional particles, nucleons or small nuclear clusters, are rare. Reasons for the inhibition of multi-fragmentation ($M_F > 2$) processes at relatively low energies can be found[21,22,104] in the compound "bottle neck" effect imposed on the density of accessible states by important exit-channel interaction barriers.

Of specific interest in this context are neck-like structures,[105–111] the matter bridges that presumably connect temporarily the massive fission fragments or products emerging from a dissipative heavy-ion reaction. In models of low-energy fission,[31,37,112] the neck is predicted to have little mass and attain a relatively short maximum length[55,113] before snapping in one place. Theoretical estimates based on the liquid-drop model capillary stability predict[83,114,115] [55] a "magic" relation of maximum neck length (ℓ_N) to neck radius (r_N) of $\ell_N \approx 11 \cdot r_N$. Experimental evidence based on fission fragment multiplicity[116–119] and final fragment kinetic energies[31,32] supports that picture. Significant probabilities for simultaneous multiple neck ruptures, which would lead to ternary or higher-order nuclear fission, are neither predicted by theory nor experimentally observed.[119,120] This fact impedes a more detailed experimental study of necked-in nuclear shapes and their connection to the nuclear equation of state.

The above conundrum can be addressed by experimentation on complex shape evolution in dissipative heavy-ion reactions which, like fission produce mostly two massive, projectile-like and target-like, fragments. While at asymptotic times the hot primary fragments have de-excited and regained their compact ground-state shapes, the intermediate, pre-scission state displays the most interesting configurations. Its temporal evolution across the multi-dimensional potential energy landscape, its eventual disintegration mode and associated time scales should reflect the variations of internal nuclear structure and basic fermionic fluid dynamics with the balance between collective and intrinsic (thermal) excitations. Since excitation energy equilibration times in heavy-ion reactions are very fast[47] (~ 10^{-22}s), the elevated nuclear temperatures attained in dissipative heavy-ion reactions at several tens of MeV per nucleon are expected to rapidly expand the system and, in particular, soften the nuclear surface. Therefore, in these reactions, pre- and final scission shapes are expected[107,121] to be more complex than occurring in low-energy fission. Since they would reflect temperature and density dependence of the mechanical, chemical, and thermal stability of nuclear matter, searching for the potentially extended neck-like structures produced in heavy-ion reactions is of particular interest. A number of experiments[60,63,64,122,123] have already reported on unexpected breakup and splitting phenomena involving the fast-moving projectile-like fragments, results of potential relevance to the task.

The present experiment has found and studied such structures in dissipative reactions ^{48}Ca + ^{112}Sn and ^{48}Ca + ^{124}Sn at a bombarding Energy of 45 MeV/A via the observation of prompt aligned binary, ternary, and quaternary fragmentation. The following Section 2 describes briefly experimental setup and procedures. Section 3. describes some details of the kinematical analysis and provides a qualitative discussion of results. Conclusions and outlook are offered in Section 4.

II.4. 2. Experimental Procedures

The experiment was conducted at the Laboratori Nazionali del Sud (LNS) Catania/Italy. Various calibration and production beams were provided by the LNS 15-MV Tandem Van de Graaff accelerator and the K800 superconducting cyclotron, respectively. Production beams of 45 A-MeV ^{48}Ca ions were used to bombard (*630-680*) mg/cm^2-thick, self-supporting targets of isotopically enriched ^{112}Sn and ^{124}Sn targets, mounted in the center of the CHIMERA target chamber CICLOPE. The CHIMERA 4π multi-detector array covers the angular range $\{1^o \leq \Theta \leq 176^o, 0^o \lesssim \phi \lesssim 180^o\}$ with 1192 Si/CsI(*Tl*) charged-particle detector telescopes, arranged in two super structures, forward CONE and central SPHERE. The Si transmission detectors had thicknesses of $\approx 300\ \mu$. They provided particle identification in atomic number (*Z*) via the *Z*-dependent specific energy loss and *A*-dependent time of flight (*TOF*) information. The residual energy (*E*) was measured with the (3-12)-cm thick CsI(*Tl*) scintillators read out via pin diodes. For light and intermediate mass charged particles, this element also provided particle identification, utilizing a pulse shape discrimination (PSD) method involving fast and slow scintillator light output components. and *A*-dependent time of flight (*TOF*) information. The residual energy (*E*) was measured with the (3-12)-cm thick CsI(*Tl*) scintillators read out via pin diodes.

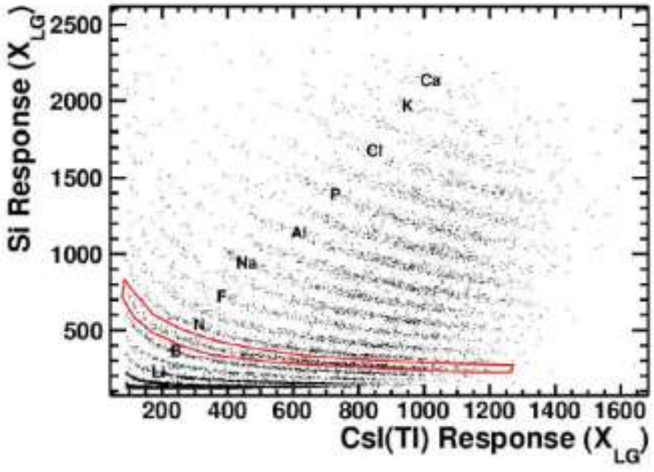

Figure 1: Events from the reaction ^{48}Ca+^{124}Sn at E/A=45 MeV. Shown is a scatter plot of Si vs. CsI response for a detector telescope at 5.2 degrees. The polygon identifies Z=6 fragment events.

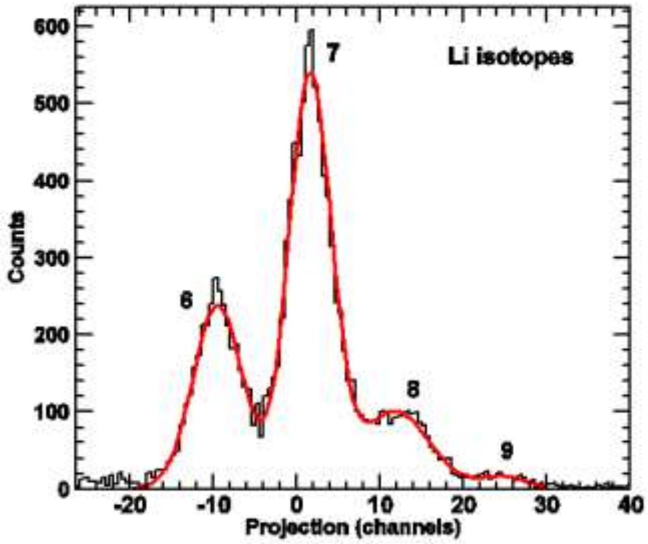

Figure 2: ^{48}Ca+^{124}Sn, isotopic distribution for Li. The yield is plotted vs. linearized continuous pseudo parameter Z-3.

The detectors were serviced by the standard, fast-slow CHIMERA electronics and data acquisition system. In the production runs, events with detected product multiplicity MF > 2 (minimum bias) were recorded, except for a concurrent, 1:20 sampling of elastic scattering events. Further details of CHIMERA detectors and electronics are presented elsewhere.[88,124] All data cited in the following presentation have been tested for instrumental bias, or corrected for finite efficiency, using a software replica[125] of the detector, which has been developed and tested extensively in the past.

An example of raw data obtained for the reaction ^{48}Ca+^{124}Sn is presented in Fig. 1. Here, the response of the Si transmission detector is plotted vs. the CsI light output in form of a scatter plot. Yield ridges are labeled according to the atomic numbers of the detected particles. The PSD method applied to the CsI(*Tl*) light output provides more precise particle identification for the lighter ions (*p*, *d*, *t*, ^{A}*He*).

In Fig. 2, the mass distribution obtained with a forward detector is plotted for element Z=3 (Li). The resolution is typical for the domain of light and intermediate-mass charged particles, commonly dubbed *IMF*s. The overall shapes of the isotopic distributions for Li to C are similar to the one depicted in Fig. 2, i.e., roughly asymmetric Gaussians. As expected, the distributions for the neutron richer target ^{124}Sn are shifted slightly to heavier masses, when compared to those for the n-poorer target ^{112}Sn.

II.4. 3. Experimental Results

II.4.3a Overall dissipative reaction features

First inspection of experimental reaction phenomena[124,125] for both systems ^{48}Ca+^{112,124}Sn reveals that, for much of the cross section, reaction phenomena are in qualitative agreement with a low-energy dissipative

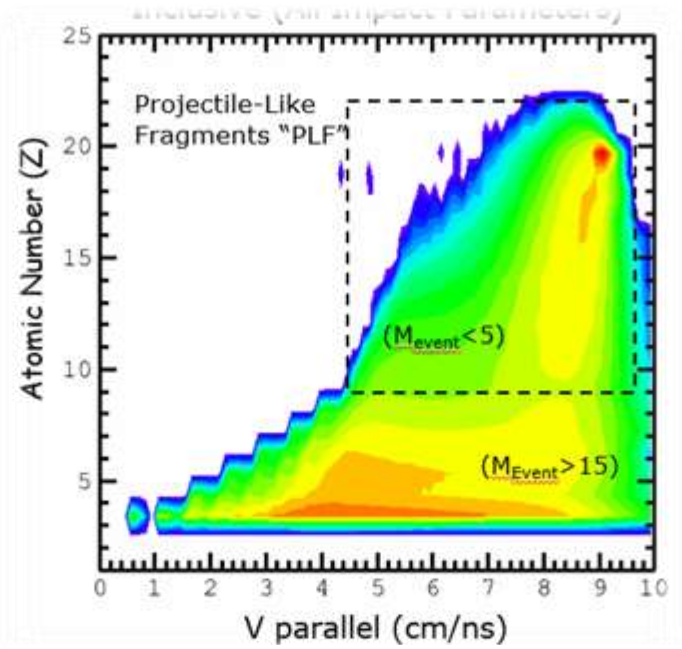

Figure 3: Atomic-number vs. velocity component in beam direction for ^{48}Ca+^{124}Sn reaction events.

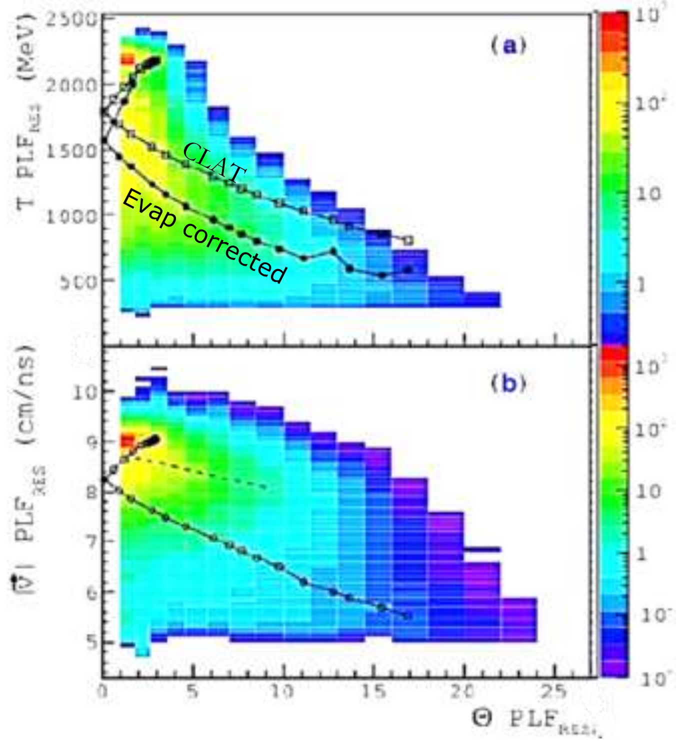

Figure 4: Wilczynski contour diagram for the reaction ^{48}Ca+^{112}Sn. Plotted are PLF lab kinetic energy (a) or speed (b) vs. laboratory emission angle $|\theta_{PLF}|$. Curves represent model calculations.

mechanism, in spite of the elevated bombarding energy of E/A=45 MeV. However, there are also striking differences, which turn out to support a different reaction scenario.

Figure 3 depicts an angle-integrated, two-dimensional, logarithmic contour diagram, where the atomic number Z is plotted vs. the velocity component in beam direction, as measured for charged particles detected in the reaction ^{48}Ca+^{124}Sn at E/A=45 MeV. The dashed enclosure defines the distribution of projectile-like fragments (PLF). It corresponds to a measured low event multiplicity of $M_{event} < 5$. The PLF distribution exhibits an intense peak of quasi-elastic and partially damped events at $\langle Z \rangle \approx 20$ and $\langle v_\parallel \rangle = 9$ cm/ns, fanning out into a ridge of yield for which reduced velocity correlates with reduced atomic number. The latter correlation is the result that might be expected from secondary particle evaporation from the hot primary PLFs.

Separated from the above PLF distribution, a domain of light and intermediate products with $Z < 10$ is observed in the contour plot of Fig. 3. The associated large event multiplicity of $M_{event} > 15$ identifies this distribution with significant levels of energy dissipation ($E_{diss} \geqslant 300$ MeV). It is noteworthy that these particles have parallel velocity components that range from low values up to that of the quasi-elastic PLFs, but not beyond.

The Wilczyński contour diagrams shown in Fig. 4 represent an effective way to visualize system trajectories. Here, the lab kinetic energy (panel ***a***) or lab velocity (panel ***b***) of PLFs are plotted vs. the corresponding emission angle θ_{PLF}, actually just vs. $|\theta_{PLF}|$. The patterns observed in Fig. 4 are also typical for dissipative reactions,[47] specifically for dissipative orbiting.[47] Here, in a collision between projectile and target nuclei, a dinuclear system is formed transiently, which rotates about its center of gravity, while kinetic energy of relative motion is dissipated. For large degrees of energy dissipation, the system has rotated past the beam direction (θ_{PLF} =

0^0), such that the PLF is emitted at negative angles. In an experiment, where positive angles are not distinguished from negative angles, one observes a superposition of the two parts of a continuous ridge of yield associated with positive and negative angles, respectively.

The curves in Fig. 4 represent averages of semi-classical model predictions obtained with the reaction code CLAT,[126] which is based on the one-body nucleon exchange model.[68] These calculations were complemented by simulations of the sequential statistical fragment decay, employing the code GEMINI.[127] As seen in Fig. 4a, the model simulations ("Evap corrected") describe the mean PLF energy-angle correlations quite well. Other inclusive observable distributions, such as the PLF mass and Z distributions, are also well reproduced by CLAT-plus-GEMINI simulations.

However, this apparent agreement of experimental data for the present Ca+Sn reactions at E/A=45 MeV with key predictions by a low-energy reaction model is deceptive. An actual discrepancy between data and theory is demonstrated by the Wilczyński plot of Fig. 4b, which changes the representation of Fig. 4a to one in which the PLF velocity, rather than its kinetic energy, is plotted vs. emission angle. Obviously, in this latter rendition (Fig. 4b), the theoretical simulation misses the experimental Wilczyński yield ridge by a significant margin, for the larger degrees of damping (negative angle ridge). In this domain, the large energy differences measured for the PLFs, relative to the beam energy, are not caused by frictional damping of the projectile velocity and subsequent particle evaporation. Rather, this kinetic energy loss must be due to a prompt loss of mass by the projectile or by the fast PLF during the nuclear interaction with the target. To recover the corresponding missing PLF mass, one is led to search the data for relatively fast, intermediate-mass fragments (IMF) that are kinematically correlated with the PLFs or their remnants. The data in Fig. 3 indicate that such IMF particles may indeed exist.

II.4.3b Multi-particle correlations in Ca+Sn reactions

In order to test the validity of the above scenario, the ^{48}Ca+^{112}Sn and ^{48}Ca+^{124}Sn data sets were scanned for events in which a Ca-like, PLF or remnant PLF_R, was detected in coincidence with intermediate-mass fragments between lithium and carbon ($3 < Z_{IMF} < 6$). The particles detected in each event were sorted according to individual Z and A values, velocity vectors, and grouped according to the overall multiplicity M_{lcp} of associated light charged particles (lcp). The latter multiplicity observable can be taken as an estimate of the collision impact parameter.[47]

Indeed, for mid-peripheral collisions ($<M_{\mathrm{lcp}}>$ ($\approx M_{event}$) $\gtrsim 15$) associated with energy losses of several hundred MeV, a significant fraction (~10%) of PLF remnants appeared in coincidence with up to 3 IMFs in the scanned mass and Z range. As indicated by the Atomic number/velocity diagram in Fig. 3, such IMF particles have a range of "mid-velocities," velocities below that of PLFs (or their remnants). This fact renders sequential, statistical evaporation from the fast-moving PLFs an unlikely origin for such IMFs.

In Fig. 5, a hypothetical scenario is shown with two IMFs placed in the spatial region between the remnants of PLF and TLF, PLF_R and TLF_R, resp. For the purpose of the specific data analysis, the reaction plane has been defined by the beam axis and the vector sum of the velocities of the two heaviest fragments, PLF_R and IMF_1, as measured in forward direction ("PLF-TLF Reference"). In a scenario, in which these latter two particles result from a dynamic splitting of a primary PLF, with a basically intact TLF, this reference would indicate the reconstructed mean direction of flight of the PLF prior to splitting.

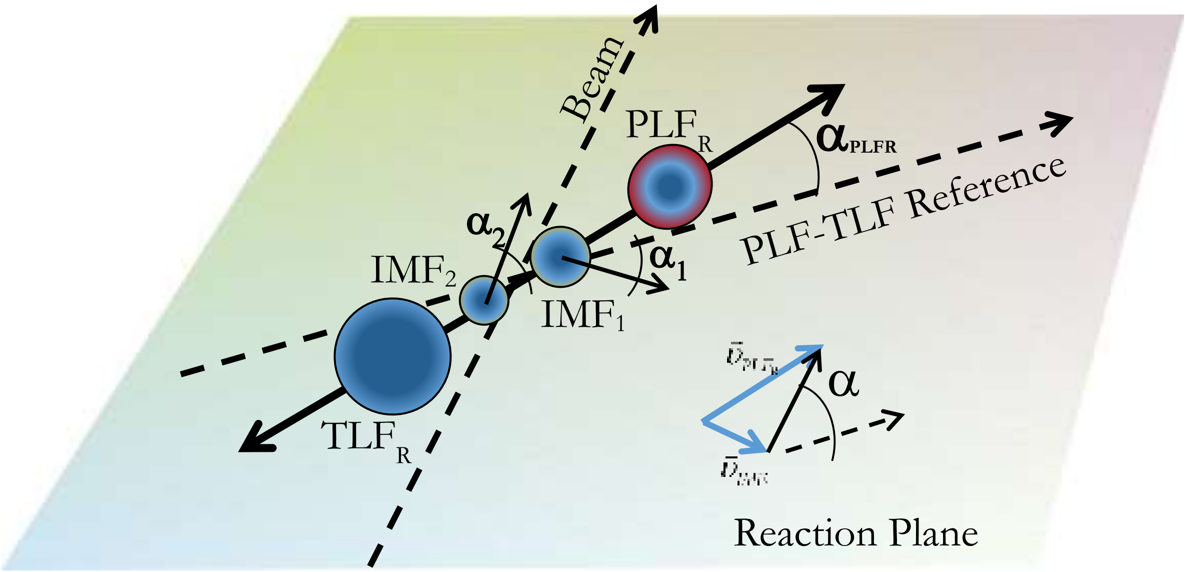

Figure 5: Schematics of reaction scenario with remnants of primary PLF and TLF and one neck-IMF in the neck region between. Dashed circle indicates relative position of second neck IMF. The reaction plane is defined by beam direction and velocity sum of PLF remnant (PLF$_R$) and correlated IMF$_1$, which approximates the initial PL-TLF separation axis. The inset defines the angle α between relative PLF$_R$-IMF$_1$ velocity vector $\vec{\upsilon}_{rel} = \vec{\upsilon}_{PLF_R} - \vec{\upsilon}_{PLF_R}$ and reference direction.

How well the reaction plane is defined by this procedure can be seen from Fig. 6 showing the out-of-plane angular distribution $dP/d\beta$ of the normalized emission probability $P \propto \sigma$, where β is the out-of-plane angle of the relative velocity $\vec{\upsilon}_{rel} = \vec{\upsilon}_{PLF_R} - \vec{\upsilon}_{IMF_1}$ vector for the PLF$_R$-IMF$_1$ pair of fragments. The resulting distribution (cf. Fig. 5) turns out to be unimodal, symmetric and peaked about $\beta = 0^0$, demonstrating the absence of bias in the procedure. A significant width of the out-of-plane distribution is expected from sequential evaporative deexcitation of hot primary reaction products.

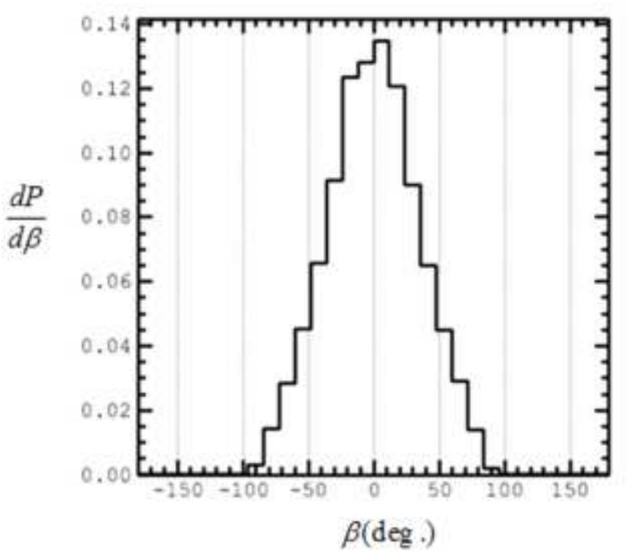

Figure 6: Out-of-plane angular correlations between PLF remnant and IMF

The orientation of the PLF remnant/IMF pair relative to the reference direction (cf. Fig. 6) in the reaction plane is illustrated in Fig. 7, where the in-plane angular distribution of the yield, dσ/dΩ$_\alpha$, is plotted vs. the angle α subtended by the relative velocity vector $\vec{\upsilon}_{rel}$ and the hypothetical PLF-TLF Reference direction. A relative angle of $\alpha < 90^0$ indicates forward emission of the PLF$_R$ and backward emission of the IMF (toward the TLF), in the relative frame of reference. For $\alpha > 90^0$, the intermediate mass fragment is emitted forward of the PLF$_R$.

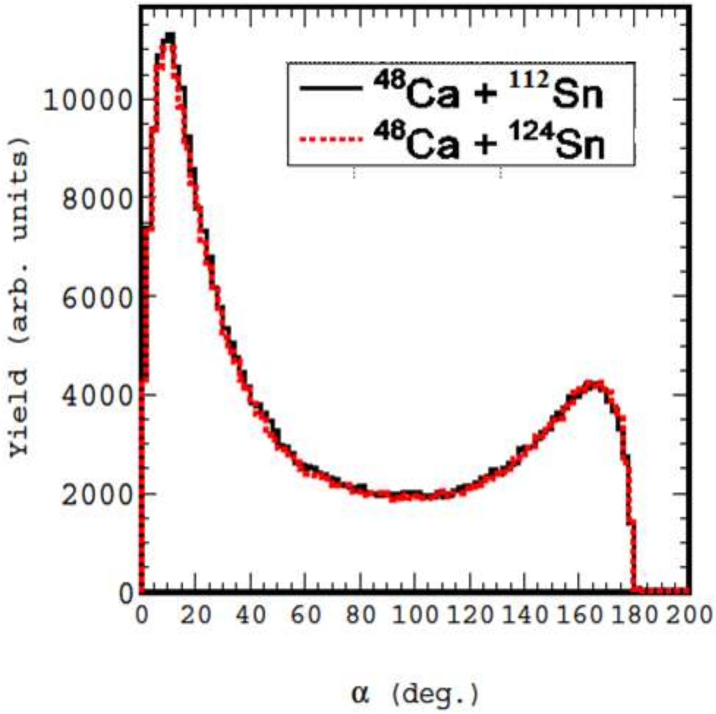

Figure 7: In-plane angular distributions $d\sigma/d\Omega_\alpha$ for light IMF-heavy PLF remnant pair, taken relative to the heavy PLF remnant, for the systems ^{48}Ca +^{112}Sn (solid-black (online) histogram) and ^{48}Ca +^{124}Sn (dotted-red (online) histogram).

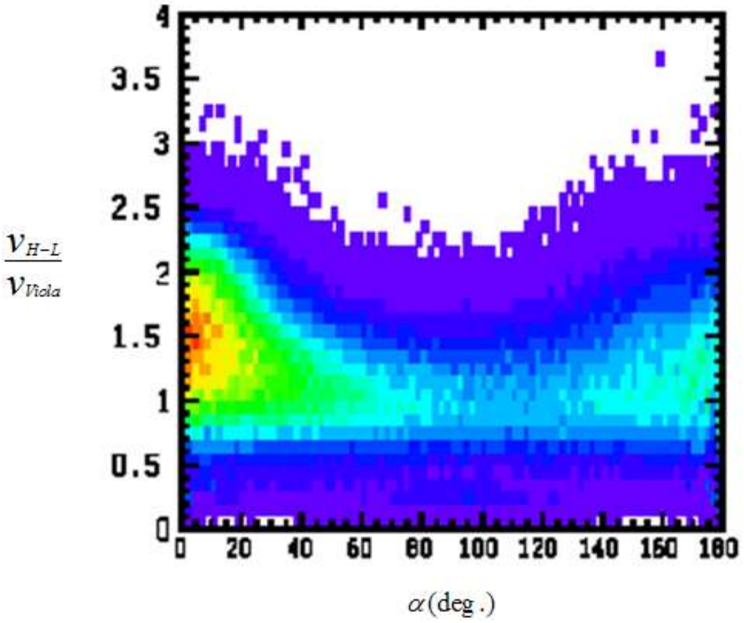

Figure 8: Contour diagram of the probability plotted vs. IMF-PLF remnant relative velocity and the in-plane orientation angle of the fragmentation axis.

Figure 7 shows the angular distribution $d\sigma/d\Omega_\alpha$ for the spatial orientation of the PLF$_R$-IMF axis, given by the relative velocity vector. The distribution is strongly anisotropic and not symmetric about $\alpha = 90^0$. It peaks strongly at forward angles and, to a somewhat lesser extent, also at backward angles. This anisotropy reflects strong alignment of the PLF$_R$-IMF axis with respect to the PLF-TLF reference (cf. Fig.5). It indicates a dominantly dynamical, non-statistical fragmentation mechanism producing the measured aligned PLF$_R$-IMF pairs. In contrast, a statistical, fission-like process would lead to a forward/backward symmetric distribution $d\sigma/d\Omega_\alpha$, and an isotropic angular distribution $d\sigma/d\alpha \approx$ const. Maximum contribution by a possible statistical component can be estimated from the backward peak in $d\sigma/d\Omega_\alpha$ amounting to a fraction of < 25% of the considered class of events.

A dominantly dynamic mechanism for the observed PLF$_R$-IMF correlations is corroborated by the measured distribution of relative velocities between the PLF remnant and the associated IMF presented in Fig. 8. Here, the yield is plotted in terms of a contour diagram vs. orientation angle α and relative velocity $\upsilon_{rel}/\upsilon_{Viola}$, normalized to the corresponding Coulomb velocity,[128]

$$\upsilon_{Viola} = \sqrt{\frac{2}{\mu}\left(0.755\frac{Z_{PLFR}Z_{IMF}}{A_{PLFR}^{\frac{1}{3}}+A_{IMF}^{\frac{1}{3}}}+7.3\right)} \qquad (1)$$

The above Equ. 1 predicts the relative velocity expected from just the mutual Coulomb repulsion of the PLF$_R$-IMF pairs, based on experimental fission systematics. The quantity μ is the reduced mass of the pair; Z and A notations are obvious.

As expected, the intensity pattern seen in the contour plot of Fig. 8 recalls the non-statistical angular distribution apparent already in Fig. 7. However, the fact that forward emission of the PLF_R is associated with high relative PLF-IMF velocities, exceeding those due to Coulomb repulsion by 50% or more, lends additional support to a dynamical production mechanism for these events.

For events corresponding to backward emission of the PLF_R, in the direction toward the TLF remnant, the distribution indicates a smaller mean excess velocity, one that is still 10% above the Coulomb systematics. This latter, smaller excess relative velocity could perhaps be explained by centrifugal velocity components adding to Coulomb repulsion. Collective rotation of the primary PLF corresponding to a mean angular momentum of $J \approx 30\hbar$ could explain the excess relative velocities observed for backward emission events in terms of a statistical disintegration of the primary PLF. Angular momentum transfer of this magnitude is consistent with CLAT simulations performed for the systems of interest here.

The above observations regarding the anisotropic angular distributions of yields and excess relative PLF_R-IMF velocities have been made consistently for both Ca+Sn reactions. They lead one to conclude that such fragment pairs do not result from sequential decay of hypothetical primary PLFs occurring outside the nuclear field of the other massive TLF reaction partner. Notably, the observed excess relative velocities require a dynamic "pull" by reaction partners left behind the fast PLFs.

Further elucidation of the complex reaction mechanism for the Ca+Sn reactions of interest here comes from extending the analysis to events, in which more than one IMF in the range $3 \leq Z_{IMF} \leq 6$ is detected in coincidence with a fast-moving PLF remnant. However, the probability $P(M_{IMF})$ of IMFs coincident with PLF_Rs decreases by roughly one order of magnitude per M_{IMF} unit. Although events with up to 3 of such IMFs have been identified in the Ca+Sn data sets, the low statistics for the higher multiplicities prevents detailed correlation analysis for $M_{IMF} \geq 3$. However, coincident IMF-IMF pairs {Li-Li, Li-Be, …. , C-C} have been detected with reasonable statistics, as shown in Fig. 9 presenting examples for such di-IMF data for ^{48}Ca+^{124}Sn. Here, angular distributions $d\sigma_i / d\cos\alpha_i$ are illustrated for the individual IMF_i ($i = 1,2$) in a pair of IMFs coincident with a fast-moving PLF_R., where α_i is the emission angle of IMF_i, measured relative to the

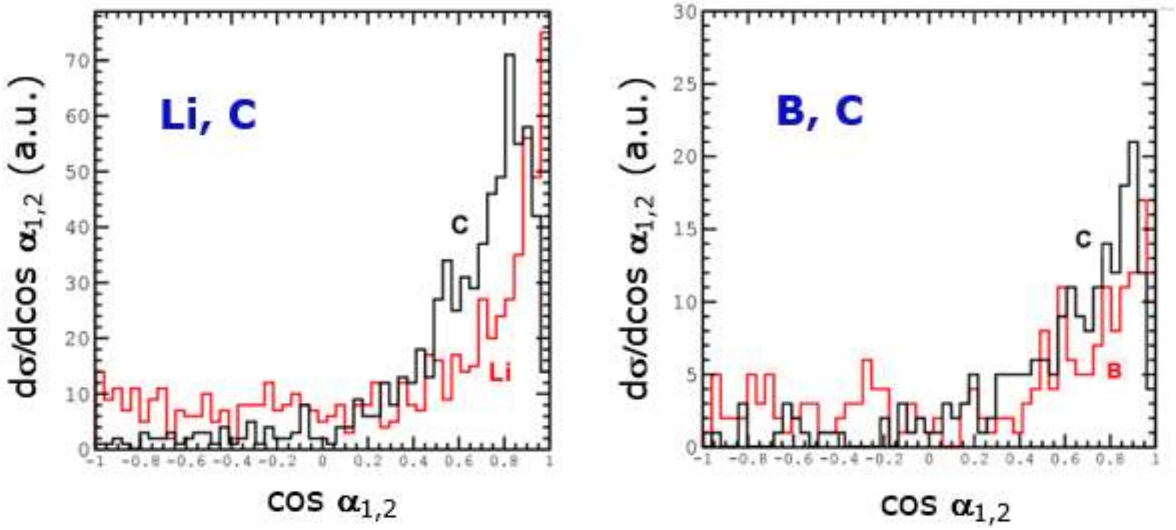

Figure 9: Correlated pairs Li-C and B-C of IMF pairs measured in coincidence with PLF_R are analyzed for the reaction ^{48}Ca+^{124}Sn. Angles are measured relative to the PLF-TLF reference (Fig. 5).

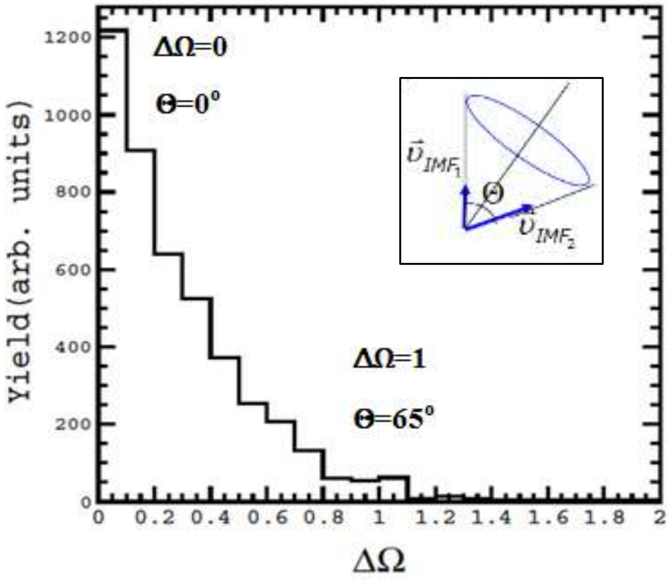

Figure 10: Correlation between emission angles of two correlated Li IMFs, measured relative to the PLF-TLF reference. The inset illustrates the angular correlation between the two IMFs, where $\Theta = \alpha_{IMF_1} - \alpha_{IMF_2}$.

PLF-TLF reference (cf. Fig. 5). Obviously, the IMF angular distributions are all anisotropic, strongly forward peaked (**cos** $\alpha_1 >$ 0) eliminating a statistical origin of these particles. The emission scenario of the IMF pair in coincidence with a PLF_R corresponds to that anticipated in Fig.5, where both IMFs are lined up, trailing behind the PLF_R. The following discussion is exemplary but concentrates on the statistically most prominent Li-Li correlations.

In order to quantify the angular correlation of the pairs of IMFs trailing the PLF_R, consider the opening angle $\Theta = \alpha_{IMF_1} - \alpha_{IMF_2}$ defined by their velocity vectors $\vec{\upsilon}_{IMF_i}\ (i = 1, 2)$. For random relative orientations of the two IMF velocity vectors, the relative probability for an actual opening angle to range below the angle Θ is given by the associated solid angle,

$$\Delta\Omega = 2\pi\left(1-\cos\left(\Theta/2\right)\right) \tag{2}$$

The corresponding un-normalized experimental probability distribution $P(\Theta)$ is plotted in Fig. 10. Obviously, this distribution is decidedly not random, since it is strongly peaked at $\Delta\Omega \approx 0$. This fact implies an approximately collinear, strongly aligned configuration of the triplets PLF_R-IMF_1-IMF_2. To appreciate the degree of alignment of the PLF_R-IMF triple, assume a mean $\Delta\Omega = (0.2\text{-}0.3)$ and recall the definition of the PLF-TLF Reference (Fig. 5) in terms of PLF_R and IMF_1. Then, the velocity vector of the second IMF is measured to be misaligned with the PLF_R/IMF_1 direction of flight by less than $\pm(15^0\text{-}\ 20^0)$.

An alternative and popular method of analyzing particle-particle correlations in terms of a velocity correlation function $R(\upsilon_{rel})$ [129–132] has also been employed to the present data for correlated Li-Li IMF pairs. Here, the coincidence yield $Y_{12}\left(\upsilon_{rel}\right)$ of correlated Li pairs, for any given relative velocity υ_{rel}, is normalized to an uncorrelated yield $\left[Y_1\left(\upsilon_1\right)\cdot Y_2\left(\upsilon_2\right)\right]_{\upsilon_{rel}}$ constructed at random out of the same data set:

$$1+R(\upsilon_{rel}) := \sum_{12} Y_{12}(\upsilon_{rel}) \Big/ \left(\frac{1}{2}\sum_{1,2} Y_1(\upsilon_1)\cdot Y_2(\upsilon_2)\right)_{\upsilon_{rel}} \tag{3}$$

This procedure is insensitive to experimental insufficiencies or artifacts.

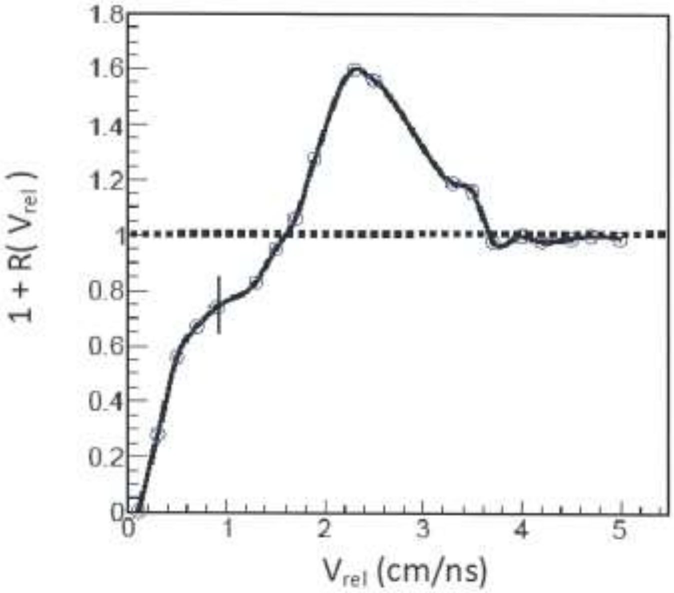

Figure 11: IMF-IMF correlation function vs. relative velocity for the two coincident IMF fragments each with Z=3. Data are for ^{48}Ca + ^{112}Sn.

The resulting correlation yield show a depression for low relative IMF-IMF velocities expected from Coulomb repulsion and a peak positive correlation at a relative velocity of $\upsilon_{rel} = \upsilon_{IMF-IMF} \approx (2.2 \pm 0.2)\, ns/cm$. This latter feature is characteristic of an attractive interaction, e.g., one associated with an intermediate system decaying into two IMFs with the above velocity. It is interesting that the above velocity is also by 10% higher than given by Coulomb systematics, but application of the corresponding formula (Equ. 1) is not justified for such light nuclei.

In order to evaluate the possibility that the two Li IMFs may originate from the decay of an excited ^{12}C intermediate,

$$^{12}C^* \xrightarrow{???} {}^{6}Li + {}^{6}Li \qquad (3)$$

statistical simulations were performed with the code GEMINI.[89] From associated particle multiplicities for such hypothetical events, a maximum excitation of a ^{12}C IMF of $E^*(^{12}C) \leq$ (24-36) MeV is expected. Carbon nuclei at such low excitations decay mostly by alpha particles and nucleons. A fission-like splitting into two Li fragments is by 3-4 orders of magnitude less likely than alpha emission. Furthermore, the two Li fragments would be directionally anticorrelated in their c.m. system. In addition, the lifetime of the C* intermediate at low excitations would be so much longer than typical nuclear interaction times[47] for the Ca+Sn reaction, such that directional correlations with the PLF would have disappeared.

These considerations further corroborate conclusions derived previously, according to which correlated IMF pairs are directly produced in the Ca+Sn heavy-ion reaction proper at mid-velocity and in the neck region. Alternative scenarios are defeated by counter arguments given above. Although a detailed analysis for IMF triplets in coincidence with PLF remnants has not been conducted for the $^{48}Ca+^{112,124}Sn$ reactions, such events have been detected in kinematical regions consistent with an extended scenario, where a significant matter bridge connecting PLF and TLF in a dissipative reaction breaks in multiple locations.

A theoretical analysis is underway investigating the potential energy landscapes and the reaction dynamics for the aligned multi-particle systems formed in Ca+Sn collisions. It turns out that mass asymmetric TLF_R-IMF-PLF_R systems are more stable in collinear configurations and, therefore, more likely formed in peripheral collisions than systems with more massive IMFs in the neck region. This fact explains naturally the observed forward/backward emission anisotropy with respect to heavier PLF_R vs. lighter IMFs. Dynamical trajectory calculations have shown that conservative forces, modeled with Coulomb and proximity nuclear forces are not sufficiently strong to account for the increased relative velocities between PLF_R and IMFs. Inclusion of dissipative forces could produce a retardation of Coulomb acceleration, in essence reproducing the apparent excess relative IMF/PLF_R velocities.

II.4.4 Conclusions

A complex, "necklace" pattern has been observed in the multi-IMF decay of neck-like structures formed transiently in ^{48}Ca+^{112,124}Sn reactions at E/A=45 MeV. The process occurs for mid-peripheral collisions, as indicated by the multiplicities of associated charged particles, and terminates the normal pattern of dissipative reactions, which still prevails in peripheral collisions. Likely, in peripheral collisions, interaction times are too short and projectile-target interpenetration too shallow, for massive necks to develop between the nuclei. In more violent, central collisions, hot matter in chaotic motion in the overlap region may not be able to reorganize into a metastable macroscopic neck.

Properties measured in this experiment pertain to masses and charges of several IMFs in a collinear configuration, aligned dynamically between PLF and TLF remnants. The estimated geometry of the neck suggests a relation between length and $\ell_N \approx (4-6) \cdot r_N$. This estimate is by approximately a factor of 2 lower than predicted by calculations[133] for the maximum neck length, before capillary instability causes its snapping. However, one has to keep in mind that these predictions have so far been made only for nuclear matter near its ground-state, while the present experiments involve matter at temperatures of approximately (2-3) MeV. Obviously, hot matter is less stable than matter in its ground state. In addition, the neck in heavy-ion reactions is subjected to mechanical stresses. It is interesting that both variables can, to some extent, be varied independently in such reactions.

More extensive measurements of the evolution of "necklace" decay patterns with excitation energy and isospin may allow one to investigate the ability of various proposed approximations of the effective equation of state of finite nuclei on their thermo-mechanical stability.

II.5. Characterization of a Novel Plastic Scintillator for γ-Rays, Neutrons, and Charged Particles

The new commercially available plastic scintillator EJ 299-33 has been fully characterized in both offline setup and in beam tests. The EJ 299-33 has been characterized in terms of n-γ separation capability using time of flight and pulse shape analysis methodologies. The plastic scintillator EJ 299-33 is observed to possess excellent n-γ pulse shape discrimination capability and have confirmed its potential value to the nuclear engineering and science community in its unique among plastic scintillators dependence of the waveform of the light pulse on the type of radiation that gave rise to this pulse. The quantitative evaluation of the n-γ separation using figures of merit suggest that the performance of EJ 299-33 is comparable to that of standard liquid scintillator NE 213 implying that replacement of liquid scintillators by EJ 299-33 plastic scintillator for applications where employing liquid scintillators is challenged by the known problems of liquids such as toxicity, flammability, high freezing points, among others is now possible.

Light output functions of EJ 299-33 have been measured for a wide range of isotopes, from hydrogen to carbon, and for a wide range of energies up to E/A = 20 MeV. A simple quadratic parameterization is provided for light output functions and is shown to fit experimental data in a manner suggesting that an extrapolation of such a parameterization over a significant energy range may be meaningful.

II. 6. A new experimental platform for exotic particle beams at the OMEGA/EP laser facility

A new method of generating energetic particle beams has been realized at the University of Rochester Laboratory for Laser Energetics (LLE). Laser-Ion Acceleration for Nuclear Science ("LIANS") at the OMEGA/EP laser facility allows experimenters to study nuclear reactions in a mode reminiscent of accelerator experiments. This platform provides intense, partially tunable beams of projectile particles with continuous, exponentially declining, spectra that can reach energies of up to tens of MeV.

The projectile particles are lifted from the near-surface region of a metallic "converter" target irradiated on the back with short-pulse laser beams, and accelerated by Coulomb fields produced by a sheath of electrons moved by the strong electromagnetic laser fields. The projectile particles can be formed as a directional beam that is used to interact with a "physics" target. So far, beams of energetic (MeV) protons and deuterons have been produced and used in direct-reaction, pickup and stripping, on targets of H, D, Li and Be.

In future experiments, yields and spectra of neutrons emitted in reactions induced by tritons will be measured as functions of mean triton energy. These will be the only triton beams available (since the 1960s) anywhere for experimentation. This technical became possible following the group's radio-chemical studies of tritium migration through metal lattices and the role of surface layers in storing tritium inventory of metallic samples. A publication of method and first results is in preparation.

III. Publications (2013-2016)

Book: *Nuclear Particle Correlations and Cluster Physics,* W. U. Schröder, Editor, World Science Publishing Co, Singapore, London, 400 pages, in press (2016)

III.1. Articles

"Radioluminescent Characteristics of the EJ 299-33 Plastic Scintillator,"
S. Nyibule, E. Henry, W. U. Schröder, J. Tõke, and the CECIL Collaboration,
Nuclear Instruments and Methods for Physics Research A 728, 36 (2013).

"Surface Boiling-An Obvious but Like No Other Decay Mode of Highly Excited Atomic Nuclei,"
J. Tõke, Invited Article, Yadernaya Phisica and Energy (English) 14 No. 2, (2013)

"Spinodal Vaporization– a Critical and Imposing Decay Mode of Highly Excited Nuclear Systems,"
J. Tõke and W.U. Schröder, Report UR-NCUR 13-030, 2013.
Physics Letters B 734, 364 (2014).

"Birks Scaling of the particle Light Output Functions for the EJ 299-33 Plastic Scintillator," by S. Nyibule, E. Henry, W. U. Schröder, J. Tõke, CECIL Collab.,
Report UR-NCUR 13-031, 2013
Nuclear Instruments and Methods for Physics Research A 768, 141-144 (2014).

"Digital Gamma-Neutron Discrimination with Organic Plastic Scintillator EJ 299-33,"
by S. Nyibule, E. Henry, J. Tõke, W. Skulski, and W. U. Schröder
Progr. Physics 10, 163 (2014).

"Dependence of Tritium Release on Temperature and Water Vapor from Stainless Steel,"
by W. T. Shmayda, M. Sharpe, A.M. Boyce, R. Shea, B. Petroski and W. U. Schröder,
Fusion Science and Technology 68, 766 (2015)

"A New Prompt Heavy-Ion Induced Fission Mode,"
by W. U. Schröder
Inv. Article, Special Edition 75 Years Fission,
Pramana, Journal for Physics, Vol. 85, pp. 227-238, (2015)

"Tritium Migration to the Surfaces of Aluminum 6061, Oxygen-Free, High-Conductivity Copper, and Stainless-Steel 316,"
by M. Sharpe, W. T. Shmayda, A.M. Boyce, R. Shea, B. Petroski and W. U. Schröder,
University of Rochester, LLE Review Vol. 141, 62-75 (2015)
Fusion Science and Technology 70, 97 (2016)

“Prompt ‘Necklace’ Fragmentation of the Dinuclear System in Dissipative Heavy-Ion Reactions,”
by O. Nyibule, M. J. Quinlan, E. Henry, H. Singh, J. Tõke and W. U. Schröder,
Inv. Paper, “Nuclear Particle Correlations and Cluster Physics,” (W. U. Schröder, Editor) ,
World Scientific Publishing Co., Singapore, London, 2016 (in press)

"Evidence for a Novel Reaction Mechanism of a Prompt Shock-Induced
Fission Following the Fusion of 78Kr and 40Ca Nuclei at E/A =10 MeV," by
E. Henry, J. Tõke, S. Nyibule, M. Quinlan, W.U. Schröder and the ISODEC Collaboration,
Report UR-NCUR 14-032, 2013, arXiv:1404.3758 (2014); To be submitted to Physical Review C, 2016

III. 2. Presentations/Lectures (2013-2016)

"Decay of Neck-Like Structures in ^{48}Ca+^{112},^{124}Sn at 45 MeV/A and their Role in Dynamical IMF Production," Gordon Research Conference in Nuclear Chemistry 2015, Colby-Sawyer College, New London, New Hampshire, USA May31 – June5 –
Invited Poster, by S. Nyibule

"Evidence for a Novel Reaction Mechanism of a Prompt Shock-Induced Fission Following the Fusion of 78Kr and 40Ca Nuclei at E/A =10 MeV," Gordon Research Conference in Nuclear Chemistry 2015, Colby-Sawyer College, New London, New Hampshire, USA May31 – June5 –
Invited Talk, by E. Henry

"Light Output and Pulse Shape Characteristics for the Novel EJ 299-3 Plastic Scintillator for Gamma-Rays, Neutrons and Charged Particles,"
2014 Symposium on Radiation Measurements and Applications, University of Michigan Ann Arbor, Michigan USA June 9 -12, 2014-Poster, by S. Nyibule

Invited Lectures given by W.U. Schröder

"Symmetry Energy: Mixed Messages from Nuclear Fragmentation,"
NuSym13, Intern. Workshop on Nuclear Symmetry Energy,
E Lansing, Michigan, July 2013.

"Proximity Splitting and Breakup in Medium Energy Heavy-Ion Reactions,"
Inv. Talk, International Workshop on Nuclear Dynamics and Thermodynamics (Honoring Joseph B. Natowitz), College Station (TX), August 2013

"Projectile Breakup following the dissipative reactions 48Ca+112Sn and 48Ca+124Sn at E/A=45 MeV," Inv. Talk. Indianapolis Meeting of the ACS, Indianapolis, IN, Sept. 2013.

"Stability of finite nuclei and the nuclear EOS,"
Inv. Talk, XXVII Texas Symp. Rel. Astrophysics, Dallas, TX, Dec. 8-13, 2013

"Heavy-Ion Induced Fission: New Prompt and Sequential Modes,"
Inv. Talk, 75-years of Nuclear Fission: Present status and future perspectives,
May 8-10, 2014, BARC, Mumbai/India.

"Nuclear stability and the equation of state,"

Inv. Seminar, Inter-University Research Centre,
New Delhi, India, May 12, 2014.

"Introduction to Nuclear Structure,"
Lecture Series at the 2014 Nuclear Chemistry Summer School, Brookhaven National Laboratory,
July 7-11, 2014, Brookhaven, New York.

"The role of ANSEL in nuclear science education at Rochester,"
Inv. Talk given at the Town Meeting on Education and Innovation in preparation of the NSAC Long Range Plan, East Lansing, Michigan, Aug. 6-8, 2014

"Shining New Light on Nuclear Reactions - High-Powered Lasers in Nuclear Experiments,"
Graduate research seminar, Univ. of Rochester, Department of Physics and Astronomy,
Rochester, Oct. 24, 2014

"EnergyScapes: Energy Policies after Fukushima,"
Guest lecture at Department of Biology, Univ. Of Rochester, Rochester, December 7, 2015

"Fusion-Fission Chips, Unusual Flavors, Dynamic nuclear instabilities in fission-like reactions,"
Colloquium, Cyclotron Institute, Texas A&M University, College Station, April 4, 2016.

III. 3. Ph.D. Theses (2013-2016)

Eric Henry:
"A Study of Primary Collision Dynamics in Inverse-Kinematics Reactions of 78Kr on 40Ca at a Bombarding Energy of 10 MeV per Nucleon,"
University of Rochester, July 16, 2015

Sheth Nyibule:
"Prompt Aligned Binary, Ternary, and Quaternary Fragmentation in 48Ca + 112Sn and 48Ca + 124 Sn Reactions at a Bombarding Energy of 45 MeV/A, and "Radioluminescence Characterization of the Novel EJ 299-33 Plastic Scintillator for γ-Rays, Neutrons, and Charged Particles,"
University of Rochester, December 9, 2015

Matthew Sharpe:
"On the Interaction of Tritium with the Surfaces of Aluminum, Copper, Stainless Steel (type 316), and Gold,"
University of Rochester, May 3, 2016

Bibliography

1. Tõke, J. & Schröder, W. U. Spinodal vaporization - a critical and imposing decay mode of highly excited nuclear systems. *Phys. Lett. B* **734,** 364–368 (2014).
2. Schröder, W. U. A new prompt heavy-ion-induced fission mode. *Pramana* **85,** 1–12 (2015).
3. Mosel, U., in *Treatise on Heavy-Ion Science* (ed. Bromley, D. A.) 3–46 (Plenum Press, 1984).
4. Umar, A. S., Oberacker, V. E., Maruhn, J. A. & Reinhard, P.-G. Microscopic description of nuclear fission dynamics. *J. Phys. G Nucl. Part. Phys.* **37,** 064037 (2010).
5. Nyibule, S. O. & Al., E. in *Nuclear particle correlations and cluster effects* (ed. Schröder, W. U.) (World Scientific Publishing Co., 2016).
6. Birks, J. *The Theory and Practice of Scintillation Counting*. (Pergamon Press, 1964).
7. Birks, J. *Photophysics of Aromatic Molecules*. (Wiley, 1970).
8. H. Müller and B. Serot., *Phys. Rev. C* **52,** 2072 (1995).
9. Wada, R. , *Phys. Rev. C* **39,** 34618 (1989).
10. Natowitz, J. , *Phys. Rev. C* **65,** 34618 (2002).
11. Shlomo, S. , *Rep. Prog. Phys.* **68,** 1 (2005).
12. Chomaz, P., Colonna, M. & Randrup, J. , *Phys. Rep.* **389,** 263 (2004).
13. Weisskopf, V. F. , *Phys. Rev.* **52,** 295 (1937).
14. Hillman, M. & Eyal, Y., 1978, unpublished. report.
15. Pühlhofer, F. , *Nucl. Phys. A* **280,** 267 (1977).
16. Gavron, A. Statistical Model Calculations in Heavy Ion Reactions. *Phys. Rev. C* **21,** 230 (1980).
17. Charity, R. J. ,.Nucl. Phys. A 483, 381
18. Tõke, J. Surface Boiling – an Obvious but like no other Decay Mode of Highly Excited Atomic Nuclei. Yad. Fisika & Energiya (Engl.), 14 No. 2, (2013)
19. Tõke, J. & Schröder, W. U. , *Phys. Rev. Lett* **82,** 5008 (1999).
20. Tõke, J., Lu, J. & Schröder, W. U., Liquid-Gas Coexistence and Critical Behavior in Boxed Pseudo-Fermi Matter. (2002), Phys. Rev. C.67, 044307 (2002)
21. Tõke, J. , *Nucl. Phys.* **A681,** 6374c (2001).
22. Tõke, J., Lu, J. & Schröder, W., Surface entropy in statistical emission of massive fragments from equilibrated nuclear systems., *Phys. Rev. C* **67,** 034609 (2003).
23. Tõke, J., Pieńkowski, L., Sobotka, L. G., Houck, M. & Schröder, W. U., Retardation of particle evaporation from excited nuclear systems due to thermal expansion. *Phys. Rev. C* **72,** 1 (2005).
24. Tõke, J. & Schröder, W. U., Common signatures of statistical Coulomb fragmentation of highly excited nuclei and phase transitions in confined microcanonical systems. *Phys. Rev. C* **79,** 1 (2009).
25. Tõke, J. & Swiatecki, W. J. , *Nucl. Phys. A* **372,** 141 (1981).
26. Rios, A., Effective interaction dependence of the liquid-gas phase transition in symmetric nuclear matter., *Nucl. Phys. A* **845,** 58 (2010).
27. Süssmann, G. , *Z. Phys. APhysik* **274,** 145 (1975).
28. Hahn, O. & F. Strassmann. , *Naturwissenschaften* **27,** 11 (1939).
29. Meitner, L. & O.R. Frisch. , *Nature* **143,** 239 (1939).
30. Bohr, N. & Wheeler, J. A. , *Phys. Rev.* **56,** 426 (1939).
31. Vandenbosch, R. & J.R. Huizenga., *Nuclear Fission.* (Academic Press, New York and London, 1973).
32. C. Wagemans. *The Nuclear Fission Process*., CRC Press, Boca Raton, London (1991).
33. Bohr, A. *, Mat.-Fys. Medd. Dan. Vid. Selsk* **26,** (1952).
34. Myers, W. D. & Swiatecki, W. J. , *Nucl. Phys* **81,** 1 (1966).
35. Cohen, S. & Swiatecki, W. J. , *Ann. Phys.* **19,** 67 (1962).
36. Cohen, S. & Swiatecki, W. J. , *Ann. Phys.* **22,** 406 (1963).
37. Moller, P. & Nix, J. , *Nucl. Phys. A* **229,** 269 (1974).
38. Cohen, S., Plasil, F. & Swiatecki, W. J., The Nuclear Rotating Liquid Drop Model. *Ann. Phys.* **82,** 557 (1974).
39. Møller, P. , *Phys. Rev. C* **79,** 064304 (2009).

40. Nilsson, S. G. , *Kgl. Dan. Vid. Selsk, Mat.-Fys. Medd* **29,** (1955).
41. Strutinsky, V. M., Shell effects in nuclear masses and deformation energies. **95,** (1967).
42. Strutinsky, V. M. , *Nucl. Phys. A* **122,** 1 (1968).
43. Brack, M., *Rev. Mod. Phys.* **44,** 320 (1972).
44. Hofmann, S. & Münzenberg, G., The discovery of the heaviest elements. *Rev. Mod. Phys.* **72,** 733–767 (2000).
45. Glässel, P. ,. *Phys. Rev. Lett* **48,** 1089 (1982).
46. Harrach, D. von. , *Phys. Rev. Lett* **48,** 1093 (1982).
47. Schröder, W. U. & J.R. Huizenga., in *Treatise on Heavy-Ion Science, Vol, 2* (ed. Bromley, D. A.) 113 (Plenum Press, 1984).
48. Moretto, L. G. & Wozniak, G. J. ,. *Annu. Rev. Nucl. Part. Sci.* **379,** (1993).
49. Hinde, D. J. *et al.* Investigating quasi-fission dynamics through mass-angle distributions. *J. Phys. Conf. Ser.* **420,** 012115 (2013).
50. Gawlikowicz, W. *et al.,* Correlations between reaction product yields as a tool for probing heavy-ion reaction scenarios., *Phys. Rev. C - Nucl. Phys.* **81,** 1 (2010).
51. Gross, D. H. E. , *Phys. Rep.* **279,** 119 (1997).
52. Gross, D. H. E., Nuclear multifragmentation, its relation to general physics : AA rich test ground of the fundamentals of statistical mechanics., *Eur. Phys. J. A* **30,** 293–302 (2006).
53. Bondorf, J. P., Statistical Multifragmentation of Nuclei., *Phys. Rep.* **133,** 133 (1995).
54. Pei, J. C. *et al.,* Deformed coordinate-space Hartree-Fock-Bogoliubov approach to weakly bound nuclei and large deformations., *Phys. Rev. C - Nucl. Phys.* **78,** 1–12 (2008).
55. Brosa, U., Grossmann, S., Müller, A. & Becker, E., Nuclear Scission. *Phys. Rep.* **197,** 167–262 (1990).
56. Colonna, M. ,. *Nucl. Phys. A* **642,** 449 (1998).
57. Baran, V., Colonna, M., Greco, V. & Di Toro, M. Reaction dynamics with exotic nuclei., *Phys. Rep.* **410,** 335 (2005).
58. Halpern, I. ,. *Annu. Rev. Nucl. Part. Sci* **21,** 245 (1971).
59. Diehl, H. & Greiner, W., Theory of ternary fission., *Nucl. Phys. A* **229,** 29–46 (1974).
60. Hudan, S. , *Phys. Rev. C* **70,** 031601 (2004).
61. Hudan, S. , *Phys. Rev. C* **71,** 054604 (2005).
62. Singh, H. *et al.* Intermediate mass fragment emission and iso-scaling in dissipative Ca+Sn reactions at 45 AMeV. Proc. Int. Conf. Recent Trends in Nucl. Phys., AIP Conf. Proc. 1524, 252 (2013).
63. Skwira-Chalot, I. *et al.* Fast ternary and quaternary breakup of the Au197+Au197 system in collisions at 15MeV/nucleon., *Phys. Rev. Lett.* **101,** 1–5 (2008).
64. De Filippo, E. *et al.,* Dynamical fission in Sn124+Ni64 collision at 35A MeV., *Phys. Rev. C - Nucl. Phys.* **71,** (2005).
65. M. DasGupta et al. ,. *Annu. Rev. Nucl. Part. Sci* **48,** 401 (1998).
66. Back, B. B., Esbensen, H., Jiang, C. L. & Rehm, K. E., Recent developments in heavy-ion fusion reactions., *Rev. Mod. Phys.* **86,** 317–360 (2014).
67. Blocki, J., Randrup, J., Swiatecki, W. J. & Tsang, C. F., One Body Dissipation. *Ann. Phys.* **105,** 427 (1977).
68. Randrup, J. , *Nucl. Inst. Meth.* **146,** 213 (1977).
69. Berger, G. F., Girod, M. & Gogny, D., *Comp. Phys. Comm.* **63,** 365 (1991).
70. Swiatecki, W. J., Siwek-Wilczynska, K. & Wilczynski, J., *Phys. Rev. C* **71,** 014602 (2005).
71. Birkelund, J. R., Tubbs, L. E., Huizenga, J. R., De, J. N. & Sperber, D., Heavy-ion fusion: Comparison of experimental data with classical trajectory models., *Phys. Rep.* **56,** 107–166 (1979).
72. Koonin, S. E., Time-dependent Hartree-Fock calculations for 16O + 16O reactions., *Phys. Lett. B* **61,** 227–230 (1976).
73. Koonin, S. E. & Davies, K. T. R. , *Phys. Rev. C* **15,** 1359 (1977).
74. Krieger, S. & Davies, K., Time-dependent Hartree-Fock calculations of fusion cross sections for the reactions 16O + 16O and 40Ca + 40Ca., *Phys. Rev. C* **18,** 2567–2573 (1978).
75. Krieger, J. , *Phys. Rev. C* **24,** 928 (1981).
76. Umar, A. S., *J. Phys. G. Nucl. Part. Phys.* **37,** 064037 (2010).

77. Umar, A. S., Oberacker, V. E. & Horowitz, C. J., Microscopic sub-barrier fusion calculations for the neutron star crust., *Phys. Rev. C* **85,** 1–8 (2012).
78. Becke, A. D. , *J. Chem. Phys.* **98,** 5648
79. Beck, A. D. , *J. Chem. Phys.* **140,** 18A301 (2014).
80. Diaz-Torres, A., *Nucl. Phys. A* **652,** 61 (1999).
81. Diaz-Torres, A., *Phys. Rev. C* **74,** 064601 (2006).
82. Nörenberg, W., *Nucl. Phys. A* **409,** 191 (1983).
83. Bertsch, G. F. & Mundinger, G.,. *Phys. Rev. C* **17,** 1646 (1978).
84. Tõke, J. & Schröder, W. U., *Phys. Rev. Lett.* **82,** 5008 (1999).
85. Toke, J. & Schröder, W. U., Spinodal vaporization - a critical and imposing decay mode of highly excited nuclear systems., *Phys. Lett. B* **734,** 364–368 (2014).
86. Quinlan, M. J. , University of Rochester, *Ph. D. Thesis* (2012).
87. Henry, E. *et al.,* Evidence for a Novel Reaction Mechanism of a Prompt Shock-Induced Fission Following the Fusion of 78Kr and 40Ca Nuclei at E/A= 10 MeV. Report UR-NCUR 14-032, 2013, arXiv:1404.3758 (2014).
88. Pagano, A ., *Nucl. Phys. A* **734,** 504 (2004).
89. Charity, R. J., *Nucl. Phys* **483,** 381 (1988).
90. Tõke, J., Surface Boiling of Highly Excited Nuclei. 12–17
91. Greiner, W., *Nuclear Physics: Present and Future.* (Springer Verlag, 2015).
92. *75 Years of Nuclear Fission.* (Indian Academy of Sciences, 2015).
93. W. D. Myers., *Droplet Model of Atomic Nuclei.* (IFI/Plenum, 1977).
94. Møller, P., Nix, J. R., Myers, W. D. & Swiatecki, W. J. Nuclear Ground-State Masses and Deformations., *Atomic Data and Nuclear Data Tables* **59,** 185–381 (1995).
95. Tõke, J. & Schröder, W. U., Liquid drop model and quantum pressure resisting noncompact nuclear geometries., *Phys. Rev. C* **65,** 044319 (2002).
96. Bohr, A. & B.R. Mottelson., *Nuclear Structure I.* (Benjamin, 1969).
97. Bohr, A. & B.R. Mottelson., *Nuclear Structure II.* (Benjamin, 1975).
98. Nilsson, S. G. & Ingemar Ragnarsson., *Shapes and Shells in Nuclear Structure.* (Cambridge University Press, 1995).
99. Krappe, H. J. & Pomorski, K., *Theory of Nuclear Fission.* (Springer Verl., 2012).
100. Walker, P. & Dracoulis, G., Energy traps in atomic nuclei. *Nature* **399,** 35–40 (1999).
101. Patyk, Z., Sobiczewski, A., Armbruster, P. & Schmidt, K. H., Shell effects in the properties of the heaviest nuclei, *Nucl. Physics, Sect. A* **491,** 267–280 (1989).
102. Tassan-Got, L. & Stephan, C., A way to dissipate energy and angular momentum for reactions in the Fermi energy domain., *Nucl. Phys. A* **524,** 121–140 (1991).
103. Swiatecki, W. J., Second UN Conf. Peaceful Uses of Atomic Energy. in 651 (1958).
104. Tõke, J. & Schröder, W. U. New Type of Shape Instability of Hot Nuclei and Nuclear Fragmentation. **2,** 5–8 (1999).
105. Brosa, U., *Nucl. Phys. A* **502,** 423c (1989).
106. Diehl, H. & Greiner, W., Theory of ternary fission in the liquid drop model. *Nucl. Phys. A* **229,** 29–46 (1974).
107. Baran, V., Colonna, M. & Di Toro, M., Neck fragmentation reaction mechanism. *Nucl. Phys. A* **730,** 329–354 (2004).
108. Toke, J. *et al.,* Intermediate-mass fragment decay of the neck zone formed in peripheral 209Bi+136Xe collisions at Elab/A=28 MeV., *Phys. Rev. Lett.* **75,** 2920–2923 (1995).
109. Montoya, C. P. *et al.,* Fragmentation of necklike structures., *Phys. Rev. Lett.* **73,** 3070–3073 (1994).
110. Verde, G., Chbihi, A., Ghetti, R. & Helgesson, J. Correlations and characterization of emitting sources. *Eur. Phys. J. A* **30,** 81–108 (2006).
111. Kurniadi, R., Perkasa, Y. S. & Waris, A. Neck curve polynomials in neck rupture model. AIP Conf. Proc. 1448, 291–296 (2012). doi:10.1063/1.4725467
112. Cârjan, N., Sierk, A. J. & Nix, J. R., Effect of dissipation on ternary fission in very heavy nuclear systems., *Nucl. Physics, Sect. A* **452,** 381–397 (1986).

113. Brosa, U. ,. *J. Phys. G. Nucl. Part. Phys.* **10,** 933 (1984).
114. Bertsch, G. F. & Das Gupta, S., A guide to microscopic models for intermediate energy heavy ion collisions., *Phys. Rep.* **160,** 189–233 (1988).
115. Bonasera, A., Heavy-ion dynamics from the point of view of classical mean-field theory., *Nucl. Physics, Sect. A* **439,** 353–370 (1985).
116. Vandenbosch, R. & Huizenga, J. R., *Nuclear Fission.* (Academic Press, 1973).
117. Gönnenwein, F., Mutterer, M. & Kopatch, Y. Ternary and quaternary fission., *Europhys. News* **36,** 11–15 (2005).
118. Brandt, R. Ternary Fission., *Angew. Chemie* **24,** 043 (1971).
119. Poenaru, D. N., Gherghescu, R. A. & Greiner, W. Complex fission phenomena., *Nucl. Phys. A* **747,** 182–205 (2005).
120. Vermote, S. *et al.,* Ternary and triton emission in the spontaneous fission of 244Cm, 246Cm and 248Cm and in the neutron induced fission of 243Cm, 245Cm and 247Cm., *Nucl. Phys. A* **806,** 1–14 (2008).
121. Di Toro, M., Olmi, A. & Roy, R. Neck Dynamics., *Eur. Phys. J. A* **30,** 65–70 (2006).
122. Filippo, E. D. E. *et al.,* How to calibrate the time scale of emission of intermediate mass fragments, *Int. Jour. Mod. Phys.* **14,** 353–357 (2005).
123. Colin, J. *et al.,* Dynamical effects in multifragmentation at intermediate energies., *Phys. Rev. C* **67,** 064603 (2003).
124. Nyibule, S. O. et al., Prompt Aligned Binary, Ternary, and Quaternary Fragmentation in 48Ca + 112Sn and 48Ca + 124 Sn Reactions at a Bombarding Energy of 45 MeV/A., Ph.D. Thesis, Univ. Rochester (2016), unpublished.
125. Quinlan, M. J. *,* Non-Equilibrium Splits of the Projectile and the Mechanism of Ca+Sn Reactions at *45 A MeV*, Ph.D. Thesis, Univ. Rochester (2011), unpublished.
126. Schröder, W. U., De Souza, R. T., Huizenga, J. R. & Schmieder, L. M. in *Nuclear Fission and Heavy-Ion-Induced Reactions* (ed. Schröder, W. U.) 255–291 (Harwood Academic Publishers, 1987).
127. Charity, R. J. GEMINI. *Phys. Rev. C* **82,** 014610 (2010).
128. Viola, V. E. & Kwiatkowski, K., Systematics of fission fragmetn tottal kinetic energy release., *Phys. Rev. C* **31,** 1550–1552 (1985).
129. Koonin, S. E., Proton pictures of high-energy nuclear collisions., *Phys. Lett. B* **70,** 43–47 (1977).
130. Yano, F. B. & Koonin, S. E., Determining Pion Source Parameters in Relativistic Heavy-Ion Collisions. *Phys. Lett. B* **78,** 556–559 (1978).
131. Knoll, J. & Randrup, J., Proton-proton correlations in high-energy nuclear collisions. *Phys. Lett. B* **103,** 264 (1981).
132. Pratt, S. & Tsang, M. B., Viewing the liquid-gas phase transition by measuring proton correlations, *Phys. Rev. C* **36,** 2390–2395 (1987).
133. Brosa, U., Grossmann, S., Müller, A. & Becker, E., Nuclear scission. *Nucl. Physics A* **502,** 423–442 (1989).
134. Umar, A. S. & Oberacker, V. E., *Private Commun.* (2014).